Earth's Future

RESEARCH ARTICLE
10.1029/2025EF006503

Long-Term Snow Avalanche Trends in High Mountain Asia: Climatic Drivers and Impacts

Arnaud Caiserman[1], Roy C. Sidle[1], Jakob Steiner[2,3], and Evgenii Shibkov[1]

[1]Mountain Societies Research Institute, University of Central Asia, Khorog, Tajikistan, [2]Institute of Geography and Regional Science, University of Graz, Graz, Austria, [3]Asian Mountain Academic Alliance, Lalitpur, Nepal

Key Points:

- Sixty million avalanches were mapped in the High Mountains of Asia over 33 years using Landsat archives
- Nearly 20% of buildings in High Mountain Asia (HMA) face frequent nearby avalanches; 22% of roads are blocked yearly, risking homes and village access
- The number of avalanches per year rose in 15% of the catchments in western HMA, due to wetter snowpack conditions and warmer temperatures

Supporting Information:

Supporting Information may be found in the online version of this article.

Correspondence to:

A. Caiserman,
arnaud.caiserman@ucentralasia.org

Citation:

Caiserman, A., Sidle, R. C., Steiner, J., & Shibkov, E. (2026). Long-term snow avalanche trends in High Mountain Asia: Climatic drivers and impacts. *Earth's Future*, *14*, e2025EF006503. https://doi.org/10.1029/2025EF006503

Received 25 APR 2025
Accepted 31 JAN 2026

Author Contributions:

Conceptualization: Arnaud Caiserman, Roy C. Sidle
Data curation: Arnaud Caiserman
Formal analysis: Arnaud Caiserman, Evgenii Shibkov
Investigation: Arnaud Caiserman, Roy C. Sidle, Jakob Steiner
Methodology: Arnaud Caiserman, Roy C. Sidle, Jakob Steiner
Software: Arnaud Caiserman
Visualization: Arnaud Caiserman, Jakob Steiner
Writing – original draft: Arnaud Caiserman, Roy C. Sidle, Evgenii Shibkov

Abstract Devastating snow avalanches are frequent in High Mountain Asia (HMA) yet remain undocumented with climate change impact drivers poorly understood. Here we introduce the first record of 60 million avalanche deposits across 10,701 small catchments, compiled from 33 years of Landsat data from 1990 until 2022 using a snow index. Potential damages from avalanches in areas at risk in HMA include nearly 20% of the buildings and up to 22% of the road network annually blocked by deposits temporarily disconnecting villages from food, energy, medicine, and communication infrastructures. Across 85% of HMA, no long-term trends of deposits were detected due to variable snow and temperature during winter. Nonetheless, in 15% of the 214 larger aggregated catchments comprising HMA, the number of deposits increased by 10 every year. Multivariate analysis among these increases of deposits and winter snow and temperature parameters from reanalysis data revealed that a few areas of western HMA experienced increases in snow water equivalent (5 mm in three decades) and air temperature (2°C) contributing to the increase of avalanche activity. There, a decrease in snowfall of 50 mm, with an increase of rainfall, contributed to the formation of weak and unstable snowpacks. Most deposit trends could not be explained by snow-temperature variables because of the complex and variable interactions between avalanches and climate. These results call for an adoption of mitigation measures in HMA to address avalanche impacts on infrastructure and human lives, especially in areas where avalanche occurrence may increase with time due to climate tendencies.

Plain Language Summary Snow avalanches are dangerous hazards in mountainous regions, particularly in populated valleys of resource-poor High Mountain Asia (HMA) where homes are close to hillslopes. In HMA, avalanche occurrence and the levels of community exposure are poorly understood, contributing to casualties and damages. Analysis of historical and recent satellite imagery revealed 60 million avalanche deposits, enabling the identification of exposed houses, roads, and other critical human activities and exposures, as well as the temporal evolution of avalanche occurrence. This assessment classifies the level of exposure to important infrastructure throughout the entire HMA and informs where avalanche activity has changed with time related to recent localized climate evolutions, namely increases in rainfall, temperature, and snow water equivalent, leading to wetter and unstable snowpack conditions.

1. Introduction

Snow avalanches are frequent hazards in mountain regions globally, but their occurrence and impacts remain poorly quantified. While global fatalities are insufficiently documented, some 5,000 lives were lost from 1983 to 2015 in North America and Europe alone (Peitzsch et al., 2020; Schweizer et al., 2015; Van Tilburg et al., 2017), mainly associated with recreational activities. However, the causes of avalanche fatalities are dissimilar across global mountains, ranging from more accidents during recreation in mountainous Europe and North America to more common fatal accidents and impacts on infrastructure and livelihoods in Asia. Avalanche casualties in High Mountain Asia (HMA) have recently been estimated at more than 3,500 persons—from 50 to >100 deaths annually—due to the location of many settlements in avalanche-prone areas, while only 15% of the accidents are related to recreation (from the 1990s to 2022) (Acharya et al., 2023) compared to 90% in North America (Strapazzon et al., 2021). In HMA, when snow avalanches inflict loss of life, infrastructure and food security are also often threatened (Caiserman et al., 2022; Sidle et al., 2023). There, roads, houses, powerlines, powerplants, and public services (e.g., hospitals, schools) are frequently damaged or destroyed by these rapid onset hazards. Remote villages and towns in these regions regularly become disconnected from food, energy, medical supplies, communication infrastructure, and water services for several days or longer (Zimmermann & Keiler, 2015). Moreover, food security is threatened by snow hazards that damage croplands and kill numerous livestock every

Writing – review & editing: Arnaud Caiserman, Roy C. Sidle, Jakob Steiner

year, that is, 1902 livestock killed in 24 avalanches in HMA (Acharya et al., 2023; Sidle et al., 2023). In addition to the inherent vulnerability, mitigation infrastructure (e.g., snow sheds, net fences, trenches) is sparse in this region (Acharya et al., 2023), and generally confined to critical areas due to high construction costs, for example, 24 galleries on Anzob Pass in Tajikistan (AsiaPlus, 2019), 12 on the Rohtang Pass in India (The Tribune, 2022), and 21 on Salang Pass, Afghanistan (World Bank, 2015). This heightened risk paired with a paucity of adequate policies and relevant research underlines the need to improve avalanche mitigation measures based on historical assessments throughout HMA.

Despite the dominance of snow avalanches and the damage they inflict, knowledge of their spatial-temporal distribution, geomorphic characteristics, and evolution during the last three decades remains poorly explored in the European Alps (Bühler et al., 2019; Giacona et al., 2021; Hafner et al., 2021) and North America (Peitzsch et al., 2021), and are virtually absent throughout HMA where the greatest societal impacts occur. The use of remote sensing in avalanche detection is still relatively new (Eckerstorfer et al., 2016) and has only recently been applied to produce susceptibility maps (Bühler et al., 2022; S. Kumar et al., 2017; D. K. Singh et al., 2019; Sykes et al., 2022), models of avalanche flows (Semakova & Bühler, 2017), and inventories of deposits at catchment (Eckerstorfer & Grahn, 2021) or regional scales with historical imagery (Caiserman et al., 2022).

Globally, several studies revealed temporal changes of snow avalanches in correlation with climate trends (Gądek et al., 2017). In Tien Shan, wetter snowpacks have moved the avalanche season earlier during the last 50 years (Hao et al., 2023). In western Himalaya, an increase of avalanche frequency during the past 150 years was related to warming temperatures and wetter snow conditions (Ballesteros-Cánovas et al., 2018). Additionally, because winters with especially heavy snowfall have been observed in western China (Zhou et al., 2018), avalanche hazard may increase along with the potential damages (Strapazzon et al., 2021), especially where climate is warming (Y. Chen et al., 2016; F. Chen et al., 2023) (Central Asia and Himalayas) or becoming wetter (Y. Chen et al., 2016; Negi et al., 2021). Changes in avalanche frequency and the consequences of potential damages are thus likely linked to climate trends. However, the dynamics of avalanche occurrence and infrastructure exposure using long-term inventories have not been systematically investigated at a wider scale (Eckert et al., 2024), which is the dual aim of our study. Concurrently, snow is naturally one of the most variable precipitation parameters, as noted in the European Alps (Schirmer et al., 2022) and Rocky Mountains (Lievens et al., 2019), which makes predictions of snowfall and related hazards complex and highly uncertain (Schirmer et al., 2022). This is particularly true in the Himalaya (e.g., Nepal) where the temporal variability of snow depth was significant with measured depths from 0.8 to 1.5 m from one year to another (Lievens et al., 2019) making reliable long-term predictions almost impossible. Within Parlung Tsangpo catchment in the southeastern Tibet Plateau, the historical spatial heterogeneity of avalanches was also recognized (Wen et al., 2024). Moreover, in the Himalayas and Karakoram, annual snowfall variability is also reported as large, reaching 0.06 m yr^{-1} from 1989 to 2016 (P. Kumar et al., 2019).

Here, we present results of the first inventory of snow avalanche deposit occurrence based on 33-year Landsat-5, 7, 8, and 9 archives from 1990 to 2022 within HMA using the Snow Avalanche Frequency Estimation (SAFE) open-access script (Caiserman et al., 2022) that produces a map of the presence and absence of avalanche deposits, thereby providing spatially explicit insights into avalanche exposure for residents and infrastructure in this vast mountain region. This unique long-term data set fills a significant knowledge gap by assessing the multi-decadal evolution of avalanche deposit surface areas, locations, and occurrences, aiming to deepen our understanding of the complex interactions between climate variability and the spatial and temporal distribution of avalanches.

2. Materials and Methods

2.1. Masking of Avalanche Susceptibility Areas in HMA

Before extracting snow avalanche deposits, we selected areas susceptible to avalanche occurrence throughout HMA. The avalanche susceptibility areas are located where winters are long and snow cover persists long enough to favor snow accumulation on steep slopes. The lower threshold for slope gradient was set at ≥8° (the minimum zonal incline for avalanches from origin to runout zone, Schaerer & McClung, 2006), using the 90-m resolution digital elevation model Shuttle Radar Topography Mission in Google Earth Engine: ee.Image ("CGIAR/SRTM90_V4") (Jarvis et al., 2008) to exclude plains and wide valleys without topographic features favoring avalanches. The SRTM-90 was used instead of SRTM-30 because we computed this mask across all the basins of

HMA covering 7,095,140 km^2. In a previous study in Afghanistan, we found no differences in total avalanche deposits comparing SRTM-30 and SRTM-90 slope masks of SAFE during a 31-year period from 1990 to 2021 (Caiserman et al., 2022). Moreover, the "snow_cover" band from ERA5 Monthly ee.ImageCollection ("ECMWF/ERA5_LAND/MONTHLY_AGGR") (Sabater, 2019), modeled in the land-surface model using snow water equivalent, was used to identify pixels that were systematically under snow using a threshold of 50% of annual snow cover persistence per pixel during January each year since 1950. Therefore, snowy pixels in January (overall, the month with the largest snowpack) and steep locations (≥8°) (Schaerer & McClung, 2006) were selected as the regional scale mask of areas susceptible to avalanches.

In addition to this spatial information, the mask was also designed to distinguish the seasonality and timing of winter. Winter duration differs among basins and sub-mountain ranges due to variable atmospheric water transport patterns across elevations, latitudes, and longitudes of HMA (Curio et al., 2015). We calculated the average monthly snow cover per pixel at avalanche risk, which was selected during the month immediately before snow cover rapidly dropped below 50%, marking the end of winter and coinciding with a significant decrease in avalanche activity in 10,701 catchments delineated using the HydroSHEDS level-12 data set: ee.FeatureCollection ("WWF/HydroSHEDS/v1/Basins/hybas_12") (Lehner & Grill, 2013; Lehner et al., 2008). HydroSHEDS level-12 is the most detailed globally available shapefile data set of catchment delineation using Pfafstetter pour point codes. Both levels of catchments are represented in Figure S1 in Supporting Information S1. These susceptible regions, which comprised about 16% of the land area within all HMA, are referred to as "susceptible areas."

2.2. Granular Scale Mask for Deposit Extraction

Once the areas susceptible to avalanches and their winter timing are determined at a regional scale, we produced a granular scale mask—30-m resolution—for avalanche deposit extraction. In the development of SAFE we showed that snow avalanche deposits are detectable once the overall snow cover has melted around the avalanche deposits, since deposits are deeper and take longer to melt (Caiserman et al., 2022). Here, we improved and upgraded the SAFE script to automatically produce data at regional scales. By applying a Normalized Difference Snow Index (NDSI) threshold of 0.2–0.7 to late-winter Landsat images 5-7-8 and 9 (Figure 1), selected to detect snow at different elevations and late-winter when only deposits remain, detectable deposits located at termini of avalanche tracks, in valley bottoms, and along rivers were segregated from the snowpacks that remained on the slopes and under shaded areas which are not deposits. Valley bottoms are selected in Google Earth Engine using the Geomorpho90m open access data set projects/sat-io/open-datasets/Geomorpho90m/cti (Amatulli et al., 2020), which globally classifies geomorphometric features using the MERIT-DEM to exclude mountain ridges where deposits cannot exist.

Landsat-8 archives were further used for two other applications in the granular mask (Figure 1). We mapped water bodies, glaciers without snow cover, and permanent snow fields to exclude them from the region of interest. Avalanche deposits are only detectable if there are no other similar proximate pixels with ice, snow, or water signals. To exclude water bodies, glaciers, and permanent snow fields at a granular scale, the mean NDSI, Equation 1 was calculated from 2013 to 2022 in summer only (July-August), where Green is the green band and SWIR is Shortwave Infrared. NDSI thresholds of <0 and >0.8 were used to remove water bodies and permanent snow/glaciers, respectively.

$$\mathrm{NDSI} = \frac{\mathrm{Green} - \mathrm{SWIR}}{\mathrm{Green} + \mathrm{SWIR}} \quad (1)$$

Second, NDSI snow coverage, acting here as the snowline elevation, from 2013 until present, was used to differentiate high from low elevation deposits across various regions, based on the *late winter* map. Effectively, avalanche deposits at low elevations and on south-facing slopes will melt earlier than deposits on other aspects at higher elevations, and therefore, different timings are required. The late winter assessment informed when to distinguish high from low elevation deposits. For example, if for a given region, late winter is in June, then the mean snow cover in June is mapped and deposits outside this June coverage are considered as low elevation deposits (33 *years low* in Figure 1), and deposits within this June coverage, extracted from a later image after snow cover melt, were classified as high-elevation deposits (33 *years high* in Figure 1). Therefore, different snow

10.1029/2025EF006503

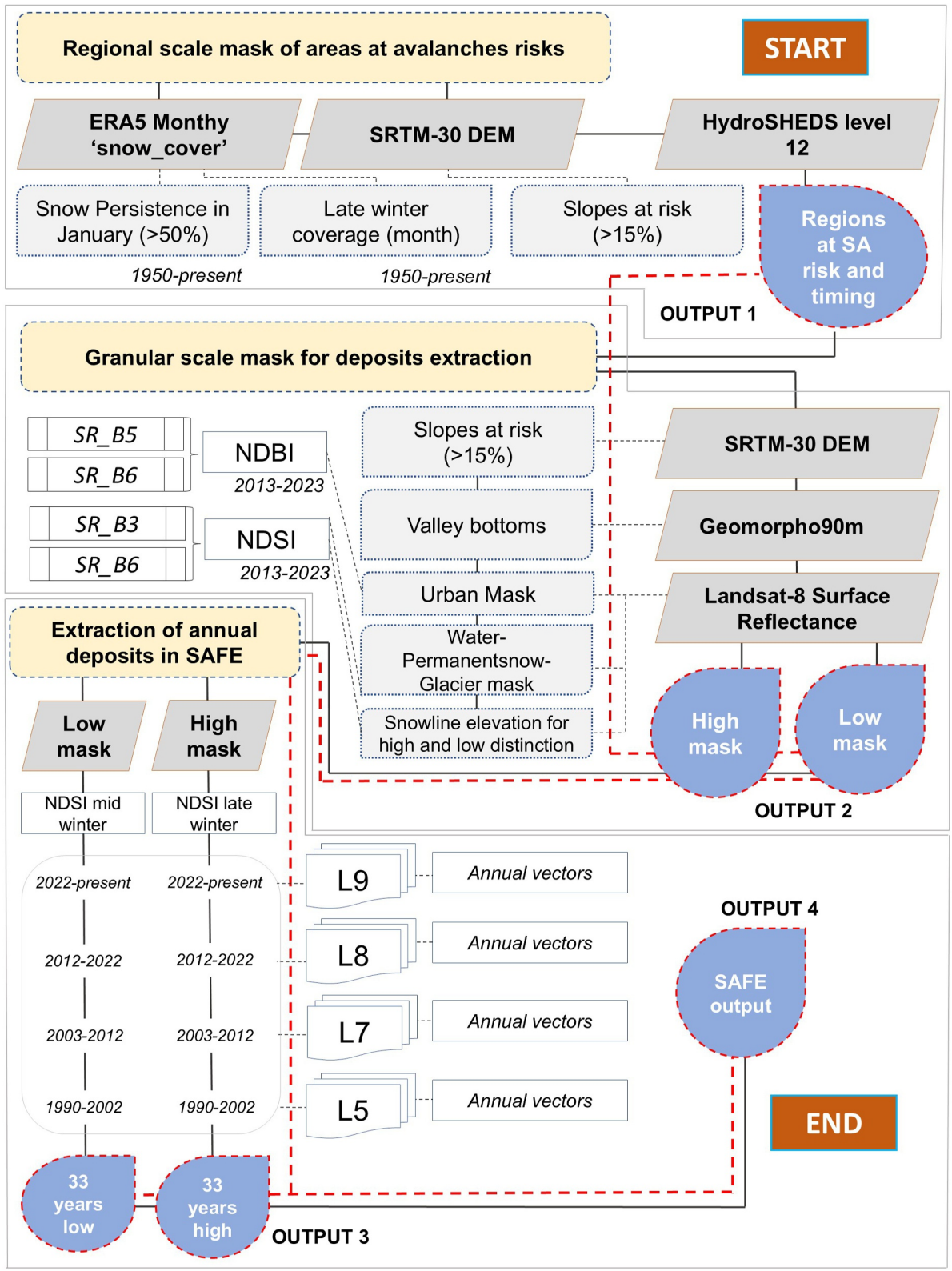

Figure 1. Flow chart of Snow Avalanche Frequency Estimation algorithm for snow avalanche deposit mapping during the past 33 years from the regional mask to granular scale (gray boxes are data inputs; light gray boxes are variables; white boxes are computed bands, indices, and shapefiles; and blue boxes are general outputs). Geomorpho90m (Amatulli et al., 2020) is the global high-resolution geomorphometric data set used here to exclude mountain ridges where deposits are not located.

cover timings are used depending on location represented by two different granular masks: one for low elevation deposits and one for high elevation deposits.

2.3. Extraction of Annual Deposits in SAFE

A summary of the overall algorithm of SAFE used here for snow avalanche deposits mapping is shown in a flow chart in Figure 1. SAFE was developed in JavaScript Google Earth Engine to enable users without powerful computational access to extract multiple years of avalanche maps online. The script was provided in the original publication where SAFE was applied in Afghanistan (Caiserman et al., 2022). High and low masks are the granular designation for high and low elevation deposit extraction. Within these two masks, SAFE calculates NDSI on images sensed after avalanche occurrences every year since 1990 at a 30 m resolution when the deposits are distinguishable from snow cover using Landsat archives (5, 7, 8, and 9 since 2022). NDSI is the most transferrable index from one version of Landsat to another and can efficiently detect snow pixels. Every annual layer is then stacked together to produce the multi-year occurrence map.

2.4. Validation of SAFE

The capacity of SAFE to accurately detect snow avalanche deposits in HMA was assessed by comparing actual deposits with automatically generated deposits in SAFE, knowing that this optical algorithm remains cloud dependent, thus locally misses short-term deposits. Since the study area is vast, we used Google Earth image archives—globally available with a spatial resolution finer than 15 m (Lesiv et al., 2018)—depending on the year and location. Unfortunately, metadata on resolution for individual images are not systematically available in Google Earth. These archives were used to identify actual snow avalanche deposits. This process consisted of manually outlining visible deposits wherever an archive image was available. The deposits visible on Google Earth were manually outlined and the corresponding SAFE yearly map was then used as a comparison. For each year and each deposit, the following protocols were employed: (a) areas of deposits identified by SAFE and overlapping the areas of deposits outlined on Google Earth images (>1% of the assessed deposit surface area overlapping the area in SAFE and the manually outlined area) were calculated and considered as true positives; (b) areas missed by SAFE compared to actual deposits were documented as false negatives; and (c) areas identified as deposits only by SAFE were recorded as false positives. The Root Mean Square Error (RMSE), Probability of Detection (POD, Equation 2), Positive Predictive Value (PPV, Equation 3) and False Discovery Rate (FDR, Equation 4) were then calculated for surface areas and number of avalanches.

$$\mathrm{POD} = \frac{\text{true positive}}{\text{true positive} + \text{false negative}} \tag{2}$$

$$\mathrm{PPV} = \frac{\text{true positive}}{\text{true positive} + \text{false positive}} \tag{3}$$

$$\mathrm{FDR} = \frac{\text{false positive}}{\text{false positive} + \text{true positive}} \tag{4}$$

2.5. Generating Exposure Maps

The outputs of SAFE are a multi-year occurrence raster with 33 annual shapefiles of deposits. This data set was superimposed on geospatial data of roads, villages (OpenStreetMap maps, 2024) and cultivated areas (Zanaga et al., 2022) in a Geographic Information System environment, within the susceptible areas to avalanche risk described previously. This area includes a total of 141,791 km of roads, 833,109 individual buildings, and 5,541 km^2 of agricultural land (Table S1 in Supporting Information S1). The total number of deposits in each size category (small, medium, and large deposits based on Jenks natural break method (Anchang et al., 2016), applied to the observed distribution of deposit surface areas) were tabulated within a 500-m buffer along each road section divided by road length (km), within a 1-km radius around each mapped building, and inside cultivated lands, reflecting typical avalanche runout distances in steep mountain terrain and capturing areas most likely to be affected by snow deposits. While the analysis in SAFE maps only residual end-of-winter deposits—without capturing full runout, wind-blown snow, and total fresh snow avalanche extent—actual avalanches in some years can reach much closer to roads and buildings than the mapped deposits suggest. The completeness and accuracy of OpenStreetMap (OSM) infrastructure data sets are steadily improving nearing a level of reliability

considered as acceptable for assessing the impacts of hazards like Glacial Lake Outburst Floods (GLOFs) on infrastructure in the HMA region as demonstrated in a recent study (F. Chen et al., 2022).

2.6. Trend Detection and Multivariate Regression Analysis Between Deposits Characteristics and ERA5-FLDAS Reanalysis Data

The 33-year trends of annual snow deposits, surface areas, and elevations were calculated for each susceptible area at avalanche risk using Mann-Kendall test on an annual basis (<0.05 p-value and $R^2 > 0.6$). To determine annual potential triggers of changes in the number, surface area, and elevation of avalanche deposits from 1990 to 2022, a multivariate regression analysis was performed in R using the ERA5 monthly aggregated data set due to its reliability (Hamm et al., 2020), especially for extreme precipitation events (M. Kumar et al., 2021), despite some overestimation of precipitation. The coarse resolution of ERA5 bands ($0.1° \times 0.1°$) enabled regional assessment of the role of each variable on avalanches. Snowfall (m/month), snow albedo (index from 0 to 1), snow cover (percentage of pixel covered by snow), and air temperature at 2 m above ground surface (Kelvin/month) were used from the ERA5 data set. November, December, January, February, and March were selected as these are the critical months for snow avalanche distribution and characteristics. Because SWE is an important determinant of snow avalanche occurrence (Stigter et al., 2017), we used a remote sensing product dedicated to SWE to estimate monthly SWE at a resolution of $0.1° \times 0.1°$: ee.ImageCollection ("NASA/FLDAS/NOAH01/C/GL/M/V001") (band SWE_inst, kg m^{-2}) across HMA (McNally & NASA/GSFC/HSL, 2018). The FLDAS SWE_inst band was generated by the FLDAS land surface model, which simulates snowpack conditions using meteorological forcings such as temperature, precipitation, and radiation to estimate the instantaneous snow water equivalent at each grid cell. Given the large set of data in the 10,701 catchments, the ERA5-FLDAS variables were aggregated into 214 larger catchments for the trend detection analysis. Moreover, for trend analysis, the original 10,701 catchments were found to be too small in surface area—averaging 109 km^2 (median: 119 km^2; standard deviation (SD): 62 km^2) to reliably encompass more than a single ERA5 pixel (which has a spatial resolution of approximately 123 km^2). It is difficult to consider any single ERA5 pixel as representative of the hydrological dynamics within those catchments. To address this issue, we aggregated the catchments from small and detailed catchments shapefiles level 12 in Pfafstetter pour point code from the WWF/HydroSHEDS v1 Basins data set ("WWF/HydroSHEDS/v1/Basins/hybas_12") to larger catchments of level 6, characterized by an average surface of 5,052 km^2 ("WWF/HydroSHEDS/v1/Basins/hybas_6"), which were large enough to cover multiple ERA5 pixels (on average, 41 pixels per aggregated catchment).

The climate variables listed previously—snowfall, snow albedo, snow cover, air temperature at 2 m, and SWE—and available from reanalysis data are the most important for avalanche formation (Greene et al., 2010). Moreover, rain-on-snow events increase SWE within a snowpack, thereby increasing avalanche risk (Peitzsch et al., 2021; Schweizer & Jamieson, 2003). Temperature at 2 m above ground surface is another key parameter because temperature variability in winter affects the nature of precipitation (liquid to solid and vice versa) and because of its influence on snowpack stability (Schweizer & Jamieson, 2003). Also, low albedo increases solar absorption in old and dirty snow, accelerates snowmelt, thereby raising the likelihood of wet snow avalanches, particularly during late winter and spring, compared to more reflective snow cover (de Scally, 1996). Therefore, snow layer temperature and albedo (reflectivity) in ERA5 were added to the analysis. In total, six variables of ERA5-FLDAS reanalysis covering a 5-month period were considered in the multivariate regression analysis.

The avalanches and ERA5-FLDAS data were aggregated in all catchments to indicate any significant trends in surface area, number of avalanches, or elevation distribution of deposits calculated previously. In the catchments with significant trends, the standardized beta coefficients to assess the relative influence of each predictor on deposit characteristics were computed in each model. Standardizing all variables allows direct comparison, as the coefficients represent the effect of a one-standard-deviation change in each predictor (ERA5-FLDAS) on the response variable (SAFE: surface area, number and elevation of deposits), especially with variables in different units. In the multivariate regression analysis, only the models with adjusted-$R^2 > 0.6$ were considered relevant in the partial explanation of deposit surface area, avalanche deposit number, or elevation changes during the last three decades. Following this selection based on the R^2 threshold in each catchment's model, the ERA5-FLDAS variables with the most significant influence (threshold p-value of 0.05) on deposits were assessed. Lastly, another Mann-Kendall trend analysis was performed on each of these variables of importance to select those which simultaneously influenced deposit characteristics and experienced significant decrease or increase with time. To estimate the rates and directions of any change per month from 1990 to 2022, data were log-transformed

to extract the Sen Slopes of each significant variable. This approach retrieves the potential impacts of the climate parameters on snow avalanche deposits detected in SAFE during the last 33 years.

2.7. Validation of ERA5 Monthly Precipitation and Temperature

Another important validation process was comparing both ERA5 monthly precipitation and air temperature at 2 m with monthly observed total precipitation and air temperature in the region. ERA5 data have been used extensively in the region and were considered adequate even in extreme settings at much higher temporal resolutions than required here (Khadka et al., 2022; Sun et al., 2023). Additionally, global monthly observation archives Global Summary of The Month (GSOM) developed by NOAA (Lawrimore et al., 2016) were used in this study during the same period SAFE was run, 1990 to 2022. Throughout 75 mountainous meteorological stations in the region from 264 to 4,701 m a.s.l., 30,000 months of air temperature data at 2 m above ground level were compared. For total precipitation, 209 stations were available in the NOAA data set (same elevation range) and 51,500 months of data were compared.

3. Results

3.1. Validation of SAFE Within the Susceptible Area to Avalanche Risks

The total surface characterized as the "susceptible area" to avalanches in HMA was 1,157,078 km^2, 16.3% of the total HMA region surveyed. Within this susceptible area to avalanches, late winter timing was mapped to select the appropriate timing of the Landsat images used in SAFE for each climatic region (Figure 2). For instance, in the upper elevations of Amu Darya and Indus (turquoise color), late winter occurs in June, while for lower elevation regions late winters occur in May, April, and March where avalanche deposits can potentially be detected. Winters ending from January to March were too short and snow cover melt is not sufficient to detect avalanche deposits in these locations.

With respect to SAFE validation, Figure 3a shows subregions where deposits were outlined in Google Earth images, ranging from Urumqi in the west to Arunachal Pradesh in the east with 22% of the outlined deposits in Balkhash, 27% in Ganga-Brahmaputra, and 51% in Indus. In total, 903 deposits were manually outlined during 9 years (Figure 3b): 2006 (15.6% of the total deposits), 2009 (1.4%), 2012 (25.3%), 2014 (3.7%), 2016 (18.1%), 2017 (11.5%), 2018 (6.6%), 2019 (2.8%), and 2022 (17.7%). SAFE accurately identified 54% of the surface areas of actual deposits outlined in Google Earth (Table 1). This correlates to a POD of 0.53 and a PPV of 0.52 (Table 1, Figures 3c and 3d), suggesting that SAFE can detect over half of the actual deposition areas present in the HMA region during the last 33 years. The percentages of areas detected by SAFE are large and non-cumulative compared to the Google Earth reference because the algorithm both underestimates and overestimates deposits relative to the manually mapped ground truth (Table 1). However, there is a risk of missing deposits due to cloud cover or shadows, which are major drawbacks of optical images. Overall, SAFE underestimated the total area outlined in Google Earth by 47%. The acquisition timing of both Landsat and Google Earth images controlled the overestimation and underestimation of deposit areas in SAFE. The underestimations occurred when the images used by SAFE for automatic deposit detection were acquired later at a time when the deposits were still visible but smaller than those observed in Google Earth images available for the same locations. Consequently, the overestimation in SAFE occurred for deposits outlined using Google Earth images acquired at an advanced stage of spring when the deposits were still visible although they had already undergone significant melting and were therefore smaller than those detected during the late-winter period in SAFE. It is important to note that this comparison is between a fully automated method—SAFE at a 30-m resolution—and a manual method with much higher precision. Concurrently, due to the medium resolution of Landsat images, SAFE inherently misses deposits with a surface area smaller than 900 m^2, which represents another limitation of the algorithm. Moreover, some deposits observed in Google Earth were smaller or missed compared with those in SAFE due to the timing of image capture. All images available in Google Earth were captured between May and July before the complete disappearance of deposits, which aligns with the timestamp of SAFE because it is not possible to distinguish deposits from snow cover in either Google Earth or SAFE when using winter images. Most importantly, the Google Earth deposits were smaller than the ones detected in SAFE due to the coarser resolution of Landsat, as suggested by the overestimation of the model: deposits detected in SAFE were overestimated compared to the total surface outlined in Google Earth by 50%, and the FDR between the total surface areas detected in SAFE and those identified in Google Earth was 0.47. While relatively high, this value is considered acceptable given the

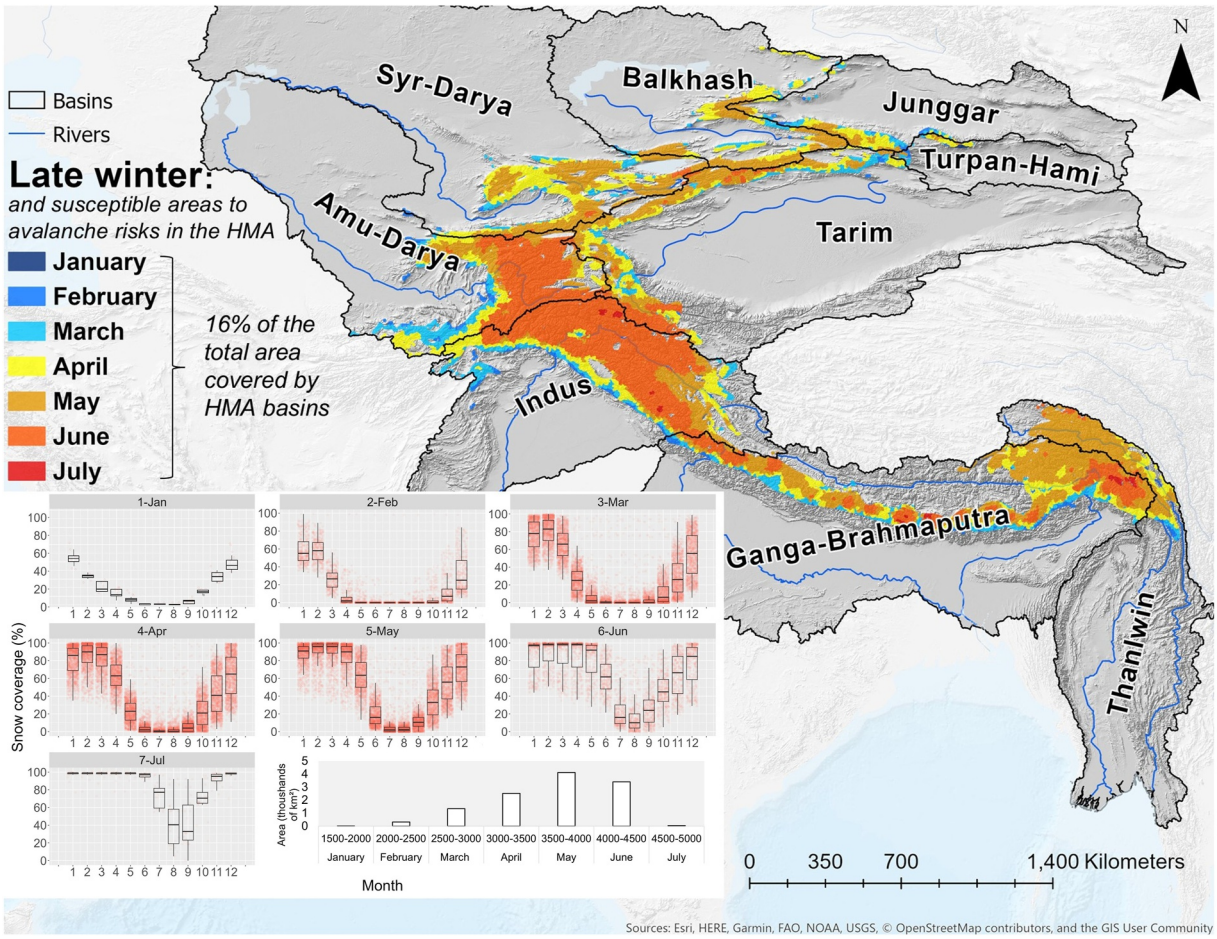

Figure 2. Spatial distribution of the late winter periods used for snow avalanche deposit detection in Snow Avalanche Frequency Estimation based on the schedule of snow coverage retrieved in ERA5. The distribution of late winter periods delineated susceptible areas to avalanche risk in High Mountain Asia. Within these areas, actual deposits were detected and the levels of exposure of infrastructure were calculated. Red dots represent all catchments within each category of late winter, predominantly observed from February to June when more catchments experience late winters. In contrast, fewer catchments fall into this category in January (very low elevations with an early end of winter) and in July (high elevations, very late winter, and spatially sparse catchments).

resolution limitations of Landsat imagery and the timing of the validation images. The RMSE between all deposits outlined in Google Earth and those automatically detected in SAFE (including those missed or overestimated by SAFE, Figure 3b) was 14,900 m^2 in Balkhash, 32,000 m^2 in Ganga-Brahmaputra, and 27,200 m^2 in Indus (Figure 3c). However, the RMSE between the deposits correctly identified by SAFE within the outlined deposits (in green in Figure 3b) and the total areas of outlined polygons (in yellow and green in Figure 3b) decreases to 5,747, 15,215, and 11,360 m^2 (Figure 3d).

Furthermore, SAFE performed well at identifying the locations of actual deposits, regardless of their surface areas. Out of 903 deposits outlined in Google Earth, SAFE correctly identified 90% of them, with a POD of 0.89 and PPV of 0.67. The FDR was 0.32, indicating that SAFE detects more deposits than are present in the validation images. This discrepancy is likely due to resolution limitations and the misinterpretation of deposits, particularly in shaded areas or on residual snowpacks. In some cases, these are not actual avalanche deposits but remnants of the snow cover which cannot be distinguished from deposits (Caiserman et al., 2022). This is more crucial than a high level of accuracy for deposit delineation because the scope of SAFE is to detect the long-term spatial patterns of avalanche occurrence by stacking yearly maps of deposits to produce the 33-year occurrence map. This implies that, while SAFE cannot perfectly match individual avalanche outlines, it is very reliable at pinpointing the locations of avalanche deposits, and highly reliable at assessing the areas covered by these actual deposits. Avalanche deposit location is one of the most important factors related to assessing community and infrastructure vulnerability.

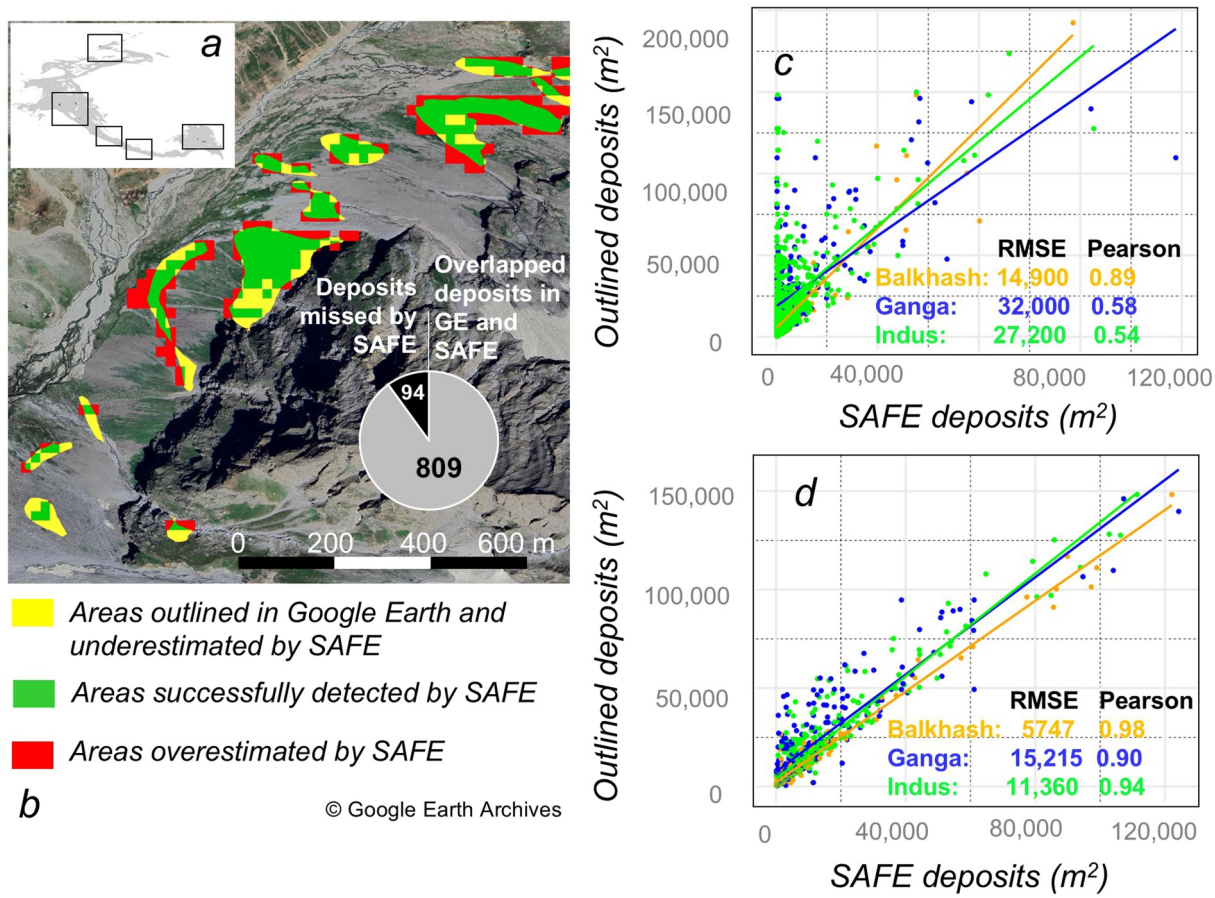

Figure 3. (a) Areas where Google Earth archives images were available to outline deposits. (b) An illustration of outlined deposits in Google Earth and Snow Avalanche Frequency Estimation (SAFE) deposits. (c) Comparison between all outlined deposits (colored in yellow, green, and red in (b)), including the deposits missed or overestimated by SAFE, and automatically detected deposits in SAFE (m^2). (d) Comparison of only deposit areas successfully detected and overlapping in both Google Earth and SAFE (overlap of at least 1% of their surface areas, colored in green in (b)).

3.2. Monthly ERA5 Accuracy in HMA

The spatial distribution of GSOM stations across HMA is presented in Figure 4a as well as the monthly SD between the observations and ERA5 predictions (Figure 4b). Additionally, the Mean Absolute Error (MAE) and the sum of squared errors for each month using MSE, which highlights the large deviations, were calculated between the two data sets (Figure 4c). Overall, the RMSE between the two variables was 49 mm and ERA5 overestimates the monthly precipitation as indicated by the monthly SDs, with a minimal error in winter. Mean

Table 1
Estimation of Snow Avalanche Frequency Estimation Performance in Assessing Surface Areas of Actual Deposits Outlined in Google Earth Archive in m^2 and Capturing the Number of Deposits Detected

Areas	Square meters	%	Number of deposits
Total areas of outlined deposits in Google Earth	15,549,414		903
Areas correctly detected by SAFE (True positive)	8,341,302	54	809
Areas underestimated by SAFE (False negative)	7,287,085	47	94
Areas overestimated by SAFE (False positive)	7,697,130	50	386
POD	0.53		0.89
PPV	0.52		0.67
FDR	0.47		0.32

10.1029/2025EF006503

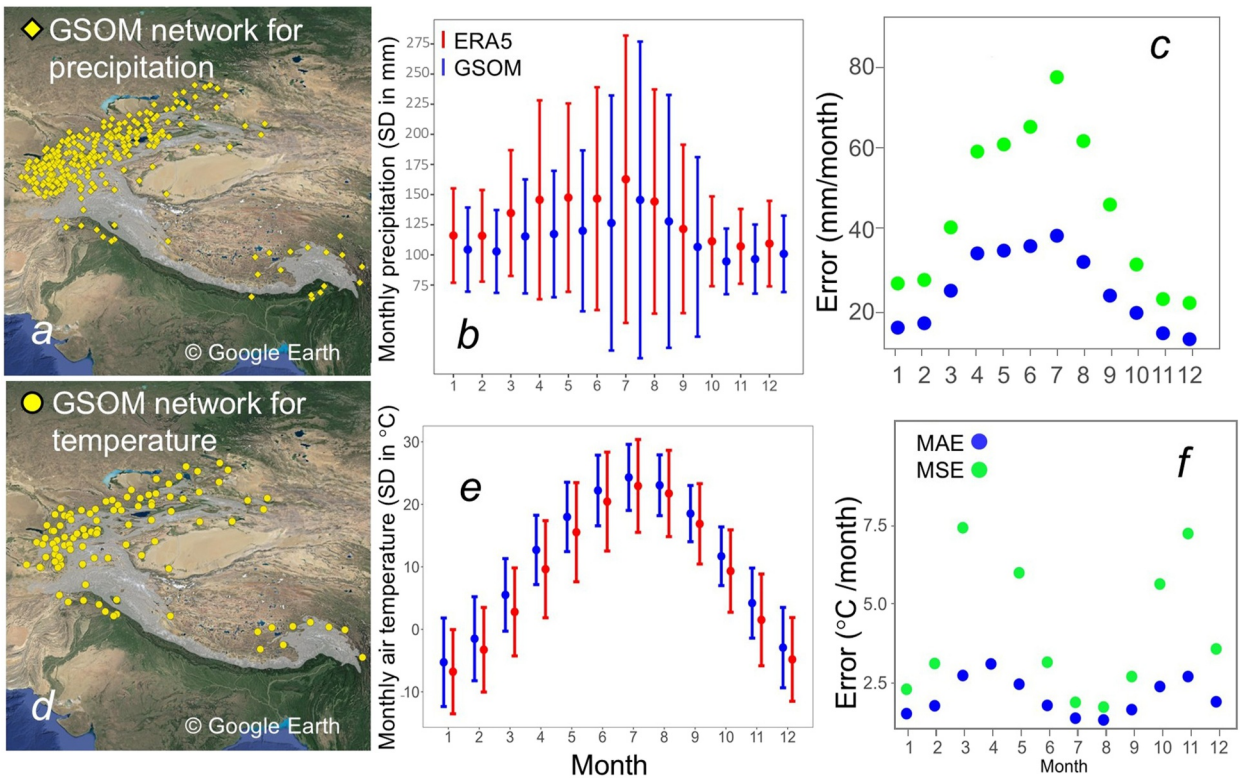

Figure 4. Comparison of temperature and total precipitation derived from ERA5 data with monthly observation archives Global Summary of The Month (GSOM) in High Mountain Asia (HMA) basins from 1990 to 2022. (a) Available stations with monthly precipitation in HMA; (b) Monthly standard deviation (SD) between ERA5 and GSOM precipitation; and (c) Monthly precipitation errors. (d) Available stations with monthly air temperature at 2 m in HMA. (e) Monthly SD between ERA5 and GSOM air temperature at 2 m, and (f) Monthly temperature errors.

Absolute Error was <10 mm in November, December, January, February and MSE was <30 mm during the same period. Errors were higher in spring with an MAE of almost 40 mm in March, April, May and June, where MSE values exceeded 50 mm. The maximum errors occurred toward late summer, July through September with MAE up to 40 mm and MSE up to 80 mm. Into autumn, the overestimations reduced somewhat with lower values of MSE and MAE (both <40 mm). Therefore, uncertainty exists in ERA5 precipitation data, especially during spring (critical season with high precipitation rates in GSOM) and summer. However, the temporal pattern of precipitation was captured by ERA5 throughout the years, with acceptable error during winter, which makes the products reliable for our study at the scale of HMA.

The same comparison was performed for monthly temperature (Figure 4d). ERA5 underestimates monthly temperature compared to GSOM data (Figure 4e). The difference between the two data sets is relatively low and uniform across the year with an annual RMSE of 3.7°C. Throughout the year, MAE is below 5°C and MSE below 10°C (Figure 4f), especially during winter and summer with less variable temperatures than during spring and fall, which makes ERA5 a reliable model for temporal distribution of air temperature at 2 m despite some significant errors.

3.3. Morphometric Characteristics of Snow Avalanche Deposits

We conducted a spatially distributed inventory of approximately 60 million snow avalanche deposits using Landsat archives (1990–2022) in SAFE (Caiserman et al., 2022) across all of HMA, separated into 10,701 individual drainage catchments. These deposits occur at the termini of runout zones and are classified by surface area as small (deposit area <5,000 m^2), medium (5,000–50,000 m^2), and large (>50,000 m^2). Throughout all periods of deposit detection, from April (early and low elevation deposits) to July (late and high elevation deposits), 71% of the detected deposits were small, 23% medium-sized, and 6% large (Figure 5). Nevertheless, small avalanches represent a significant risk as they can occur multiple times at the same location within the 33-year

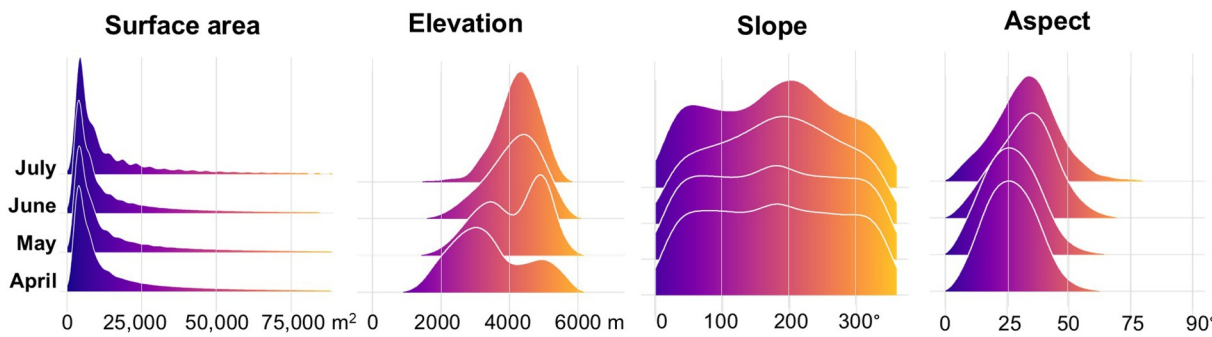

Figure 5. Geomorphic characteristics of detected deposits: surface area (m^2), elevation (m), aspect (degrees), and slope (degrees).

period of analysis. During this period, 10% of all pixels covered by small deposits were characterized by repeated occurrences of small deposits, where annual deposits were detected in more than 5 years at the same location within the 33-year period. In contrast, only 6% of large avalanches occur at the same location from 1 year to another. The surface areas of deposits detected at low elevations from late winter images in April and May (mean: 12,500 m^2) to early summer in June and July at higher elevations (12,700 m^2) are very similar, implying that the risk, based on the surface areas of individual deposits, is relatively uniform across elevation ranges.

Distinct from the uniform distribution of depositional surfaces across elevations, higher altitudes are affected by more deposits than lower elevations: 3% of all detected snow deposits occurred below 2,000 m a.s.l, 45% from 2,000 to 4,000 m, and 52% above 4,000 m. The average elevation of deposits in June and July was 4,200 m (SD: 520 m) (Figure 5), much higher than those detected earlier in the year, starting from April to May, with a mean elevation of 2,500 m (σ: 925 m). For all periods, the avalanche distribution by aspect exhibited similar patterns. Avalanches mostly occur on south facing slopes, with 42% of the deposits ranging from 112° to 247° and 28% on northeast and northwest aspects throughout HMA (Figure 5). Deposits detected at higher elevations in June and July occurred in slightly steeper terrain compared to deposits at lower elevations where year-round settlements exist. These summer deposits above 4,000 m had a mean gradient of 30° (σ: 12°) while those detected earlier (April and May) between 2000 and 4,000 m, had an average gradient of 25° (σ: 10°) (Figure 5).

3.4. Spatial Distribution of Exposure to Snow Avalanches in HMA

Avalanche deposit occurrence across HMA (Figure 6a) was analyzed by remote sensing—Landsat 5, 7, 8, and 9 archives as illustrated in Figure 6b—in the susceptible mountainous area delineated by SAFE using snow persistence, slope gradient, and valley bottoms, which constitutes 16% of the HMA terrain (see Methods). Western HMA (Amu Darya and Indus) had by far the largest proportion of high deposit occurrence (in red, >150 deposits km^{-2} yr^{-1}, >30% of the total susceptibility spatial mask covered by deposits) followed by central to northern HMA (Turpan-Hami, Tarim, Junggar, Balkhash, Syr Darya), and southeastern HMA (Ganga-Brahmaputra) all with high deposit occurrence across <30% of their susceptible areas. Thanlwin area appeared to be the least impacted by high-frequency avalanches with only 18% of the susceptible avalanche area affected. The proportions of medium frequency deposit occurrence (in orange, 51 to 150 deposits km^{-2} yr^{-1}) were much higher; in central to northern HMA (Balkhash, Syr Darya, Junggar, Turpan, and Tarim) covering more than 50% of their susceptible areas. However, areas most affected by high frequencies of avalanches (Amu Darya and Indus) were not as heavily impacted by medium occurrence avalanches and had similar proportions as southeastern HMA (Ganga-Brahmaputra, Thanlwin) with approximately 40% of their susceptible areas affected. The low occurrence category (in yellow, <50 deposits km^{-2} yr^{-1}) occupied a much smaller proportion throughout the northern and western HMA (Indus, Amu Darya, Syr Darya, Tarim, Junggar, Turpan, and Balkhash) with <27% of their susceptible areas affected. However, in southern and eastern HMA, the Ganga-Brahmaputra and Thanlwin basins were characterized by higher proportions of low frequency avalanche occurrence, 36.3% and 38%, respectively. Overall, medium occurrence deposits were most common across HMA.

By overlaying open-access infrastructure data within HMA where avalanche deposits were detected (Figure 7), it appears that Thanlwin basin, despite having a small share of high avalanche deposit occurrence (Figure 6), had the greatest avalanche exposure along roads (all deposits annually counted within a 500 m buffer along road sections

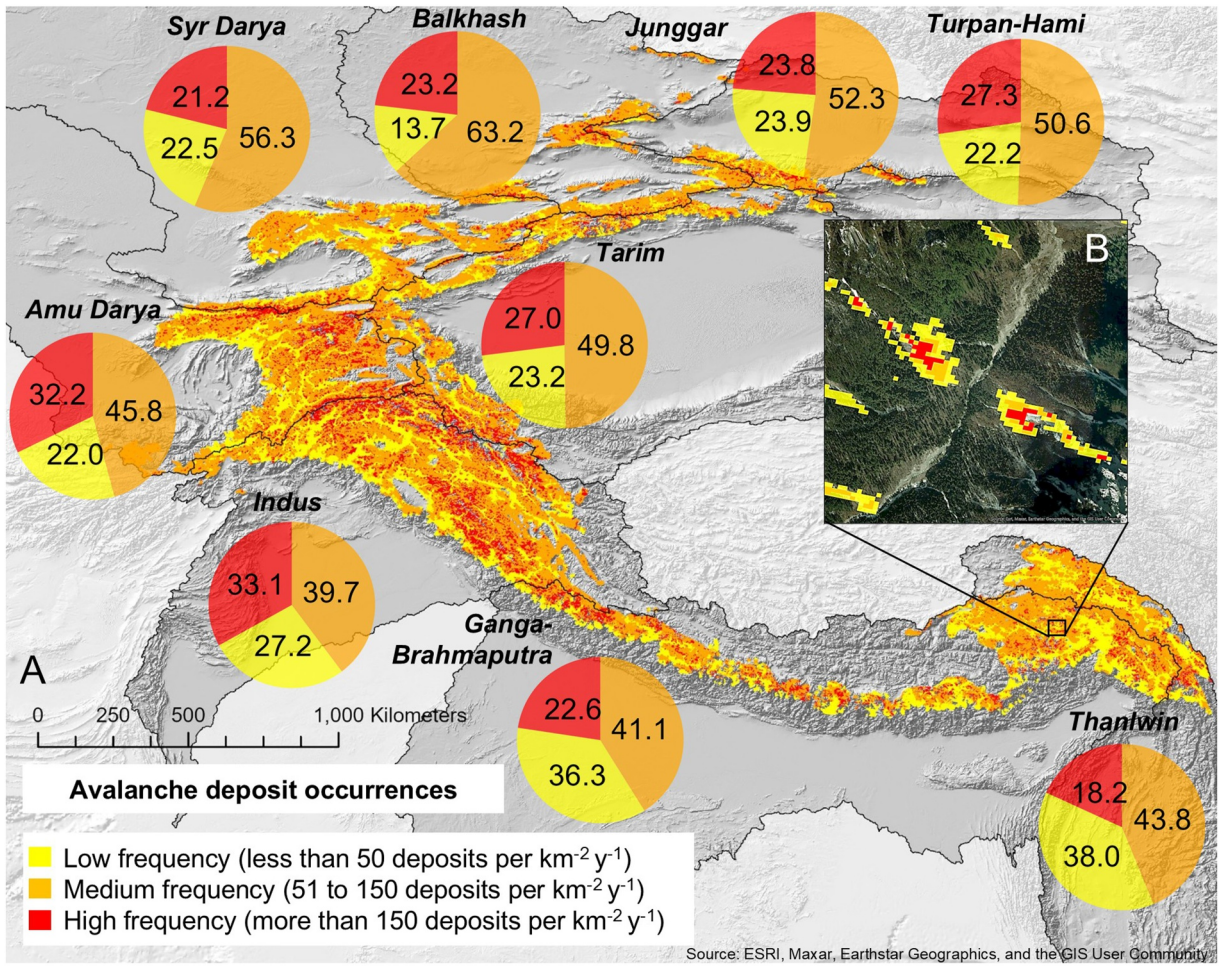

Figure 6. Snow deposit records from 1990 through 2022 in High Mountain Asia susceptible areas: (a) Overall frequencies of avalanche deposits for the susceptible area at risk in each basin. (b) An example of Snow Avalanche Frequency Estimation output in Ganga area (scale 1:500). © ESA WorldCover project 2021/Contains modified Copernicus Sentinel data (2021) processed by ESA WorldCover consortium (Zanaga et al., 2022).

km^{-1} yr^{-1}) and buildings (deposits within a 500 m radius of buildings), with 22% and 24% of roads and built-up areas in the susceptible area struck by at least one avalanche per year, respectively (Figure 7). Turpan basin, with a relatively large proportion of high-frequency avalanche deposit occurrence, had the lowest exposure due to the remote nature of infrastructure with <5% of roads and built-up areas exposed. In northwestern HMA (Junggar, Amu Darya, Tarim, Indus and Balkhash), 18%–13% of built-up areas were impacted by avalanches, every year. In contrast, <7% of built-up areas in Syr Darya and Ganga-Brahmaputra were affected by deposits. Road systems in northwestern HMA were also heavily impacted by avalanches with more than one deposit blocking road sections every year in Balkhash and followed by Tarim, Junggar, Amu Darya, and Syr Darya (in descending order from 20% to 14% of their total road distance). Roads in Indus and Ganga of southern HMA were more modestly impacted (<12% of the road distance). In addition to roads and buildings, croplands are exposed to avalanches, generally by large deposits and mostly in western HMA. In Tarim basin, 12% of the cropland was affected by ≥1 deposit km^{-2} yr^{-1} followed by Amu Darya, Syr Darya and Indus with approximately 10% of cropland affected in susceptible areas. Cropland exposure to avalanches was more modest in northern HMA (4%–7% in Balkhash and Junggar) and even lower in the south (Ganga-Brahmaputra, 2%) and extreme northeast (Turpan, 1%).

3.5. Local Avalanche Trends Amid Snow Variability

In each of these 214 catchments, a Mann-Kendall test on avalanche deposit metrics was performed—number, surface area, and elevation distribution—to assess whether these have significantly changed from 1990 to 2022. The results suggest that none of the catchments showed significant trends in surface area nor elevation distribution

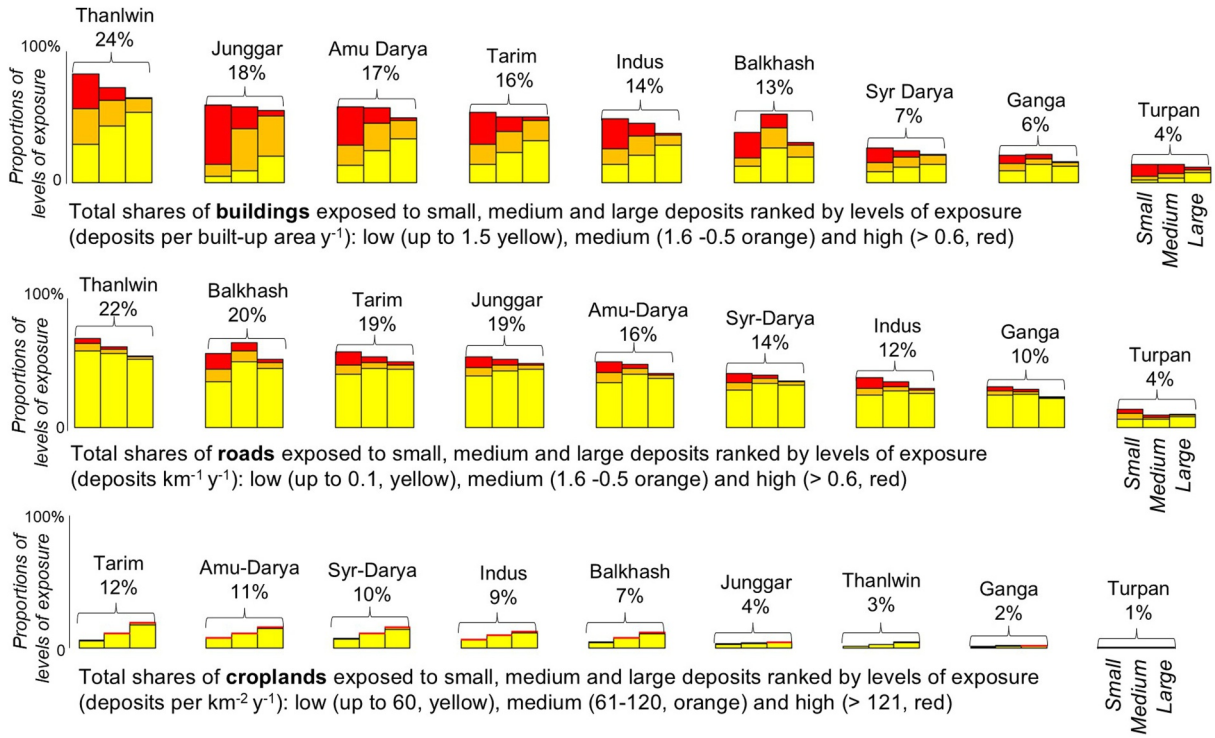

Figure 7. Distribution of small, medium, and large avalanches detected within built-up areas, road sections, and croplands.

of avalanches. The absence of any trend is largely attributed to the interannual variability of surface area and number of deposits calculated across three decades based on coefficients of variation (CV) (Figure 8a). Among all catchments, the CV of surface area of avalanches was 53% and the CV of avalanche number across years was 50%; however, the CV of mean elevation was only 5%, demonstrating the relatively even distribution of deposits along the slopes during the 33-year period. Such variabilities mask the existence of potential trends.

Based on robust statistics ($R^2 > 0.6$ and p-value < 0.05 thresholds), we found that only 33 of the 214 large catchments exhibited temporal trends in the number of avalanche deposits, but not for surface area or elevation. In these 33 catchments, only temporal increases in avalanche deposits were noted and no significant decrease occurred (Figure 8b). The average annual increase of the number of deposits in all 33 catchments was 12 new deposits per year. These occurred in western HMA (Figure 8c), southern Syr Darya (south Tien Shan in Kyrgyzstan), eastern Amu Darya (Pamir and Alay in Tajikistan and Kyrgyzstan; Hindu Kush in Afghanistan and Pakistan), central Indus (Karakoram between China, India and Pakistan), and eastern Ganga-Brahmaputra (Himadri and Ladakh in Nepal, India and Pakistan).

The absence of generalized significant trends in 85% of the 214 studied catchments is related to the effects of the variability of relevant climate parameters retrieved in ERA5 and FLDAS reanalysis products (i.e., air temperature, snowfall, snow coverage, snow albedo in ERA5 and snow water equivalent from FLDAS) to the incidence of snow avalanche deposits (Figure 8d). CVs of climate-related parameters are high: snow cover (28%), snowfall (50%) and SWE (58%). Such variabilities mask potential avalanche temporal trends. Only air temperature and snow albedo had more consistent distributions with lower variability across time, less than 1% and 11% respectively throughout HMA. The consistency of temperature seasonality was already observed in other parts of HMA (Heynen et al., 2016) and low CV of air temperature can be attributed to atmospheric stabilization mechanisms such as cold-air pooling during wintertime, which traps cold air in valleys and limits year-to-year fluctuations in temperature (Pepin et al., 2022). However, ERA5-Land tends to underestimate small-scale interannual variability due to its coarse spatial resolution, which spatially smooths local temperature extremes in complex orographic terrain (Cavalleri et al., 2024).

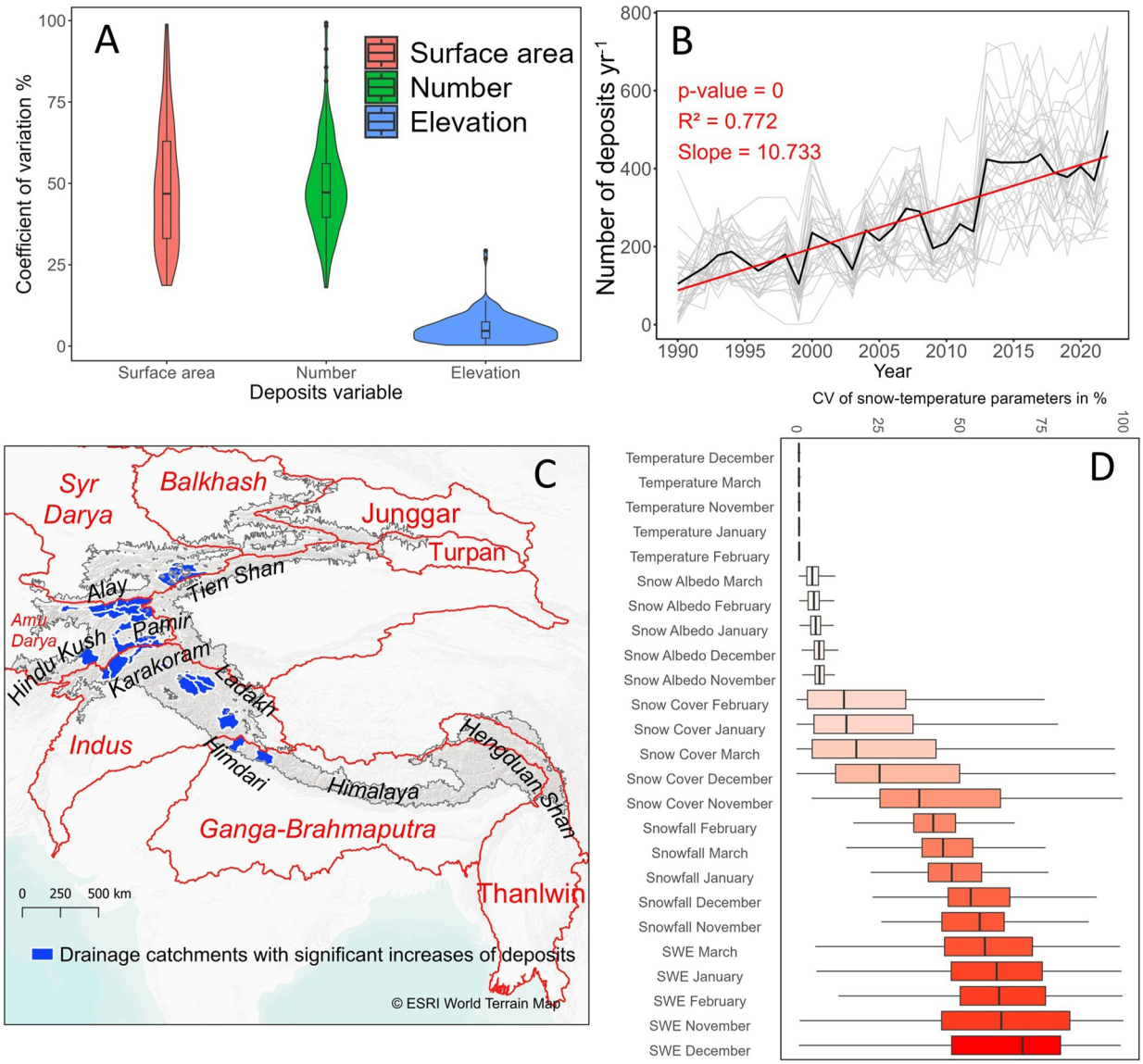

Figure 8. Evidence of increasing avalanche deposit occurrence in 33 catchments despite high variability of relevant parameters: (a) Coefficient of variation of surface area, number, and elevation distribution of avalanche deposits in all 214 catchments. (b) Significant increase of number of deposits in 33 catchments of High Mountain Asia (HMA) that exhibited significant temporal trends from 1990 to 2022 ($R^2 > 0.6$; *p-value* < 0.05). (c) Map of the catchments where the number of avalanches has increased. (d) Coefficient of variation of air temperature, snowfall, snow coverage, snow albedo, and snow water equivalent in HMA. © ESRI World Terrain Map.

3.6. Increasing Occurrence of Snow Avalanche Deposits in Central Asia Linked to Wetter and Warmer Conditions

The increase of avalanche deposits found in 15% of the study catchments is contemporaneous with widespread temperature increases across HMA (Pepin et al., 2015). To understand this relationship, a multivariate regression was conducted to examine how five snow and temperature variables affected deposit occurrence from November to March 1990–2022. Twenty-five variables each year were assessed using thresholds of adjusted-$R^2 > 0.6$ and *p*-value < 0.05 to identify the most significant factors. These results in the 33 catchments with trends in deposit numbers showed that in 18% (6 catchments), snow and temperature variables from ERA5-FLDAS reanalysis significantly explained the increase of deposits during the last three decades (Figure 9a). All these catchments are in western HMA. There was indeed a consistent relationship between the increase of air temperature and increase of avalanche deposits mapped in SAFE in the Panj (+13 deposits yr^{-1}), Wakhan (+10 deposits yr^{-1}), and Shiveh (+16 deposits yr^{-1}) catchments (Figure 9b, all Tajikistan), with standardized estimates of 0.81, 0.49 and 0.55 of

10.1029/2025EF006503

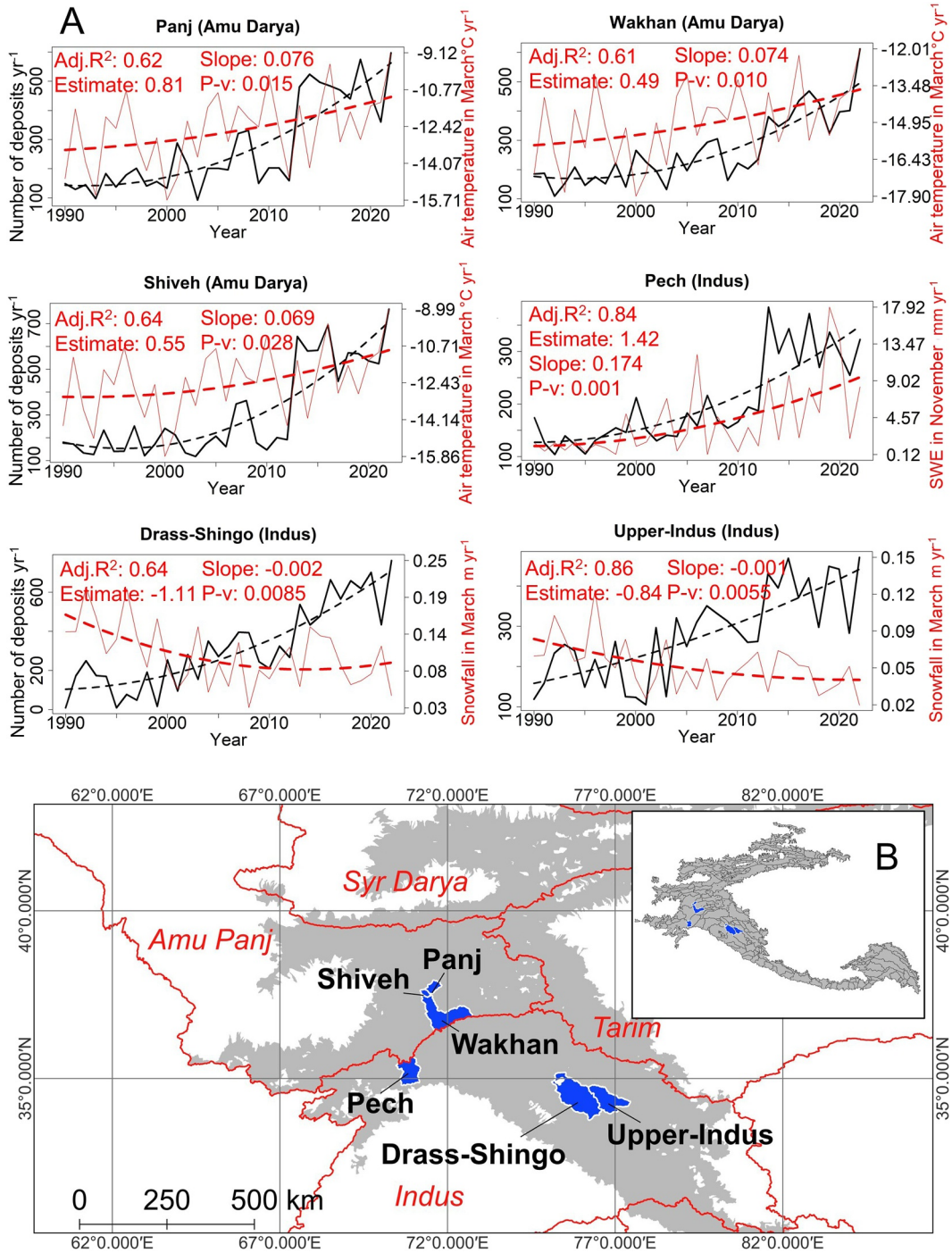

Figure 9. Localized increases of the number of avalanche deposits due to significant trends of temperature and snow variables: (a) Six catchments of western High Mountain Asia with increased numbers of avalanche deposits partially (Adj-R^2 > 0.6) explained by simultaneous significant trends in snow or temperature variables: Panj (catchment surface: 1,053 km^2), Shiveh (428 km^2), Wakhan (6,769 km^2), Pech (3,852 km^2), Drass-Shingo (10,235 km^2), and Upper-Indus (5,183 km^2)—dashed lines represent the polynomial regressions in red for weather variables and in black for number of deposits. (b) Map of the six catchments where the increase of avalanche deposit numbers could be partially explained.

air temperature SD units. According to ERA5 reanalysis, the air temperature has increased by approximately 2°C from 1990 to 2022, as similarly observed in the Pamir mountains (Vanselow et al., 2021). At similar longitudes toward the south in the Indus basin, Pech catchment (Afghanistan) exhibited an increase in SWE of almost 6 mm

from 1990 to 2022 significantly contributing to the increase in number of deposits detected in SAFE (+7 deposits yr^{-1}). Indeed, clear evidence of trends in SWE occurred in this region with the wettest snowpack conditions in February 2017. In the Indus basin, the Drass-Shingo and Upper-Indus catchments (India, Pakistan) revealed counterintuitive results where decreasing snowfall led to increases in numbers of deposits (respectively +18 and + 9 deposits yr^{-1}) with standardized estimates of −1.1 and −0.84, respectively. In these two catchments, snowfall decreased by approximately 50 mm from 1990 to 2022, according to ERA5 data. Other studies in the region indicate similar declining snowfall trends, with a shift toward increased rainfall due to rising temperatures (Dar et al., 2024). Following the results of the adjusted-R^2 in the multivariate regression analysis, the full data set of snow and temperature variables explains from 61% (Wakhan) to 86% (Upper-Indus) of the significant changes of deposit occurrence during the last three decades in these 33 catchments.

4. Discussion

4.1. Limitations

Because of SAFE's large scope and automatic detection process, our approach tends to overestimate the number and surface area of snow avalanches as indicated by an FDR of 0.32 and 0.47, respectively, when comparing SAFE-derived deposits with manually outlined ones. Therefore, the absolute values of deposit trends should be interpreted with caution. Moreover, SAFE identifies where avalanche deposits stop, highlighting high-risk areas based on historical data. Except in broad alluvial fans where deposits can spread, SAFE cannot distinguish individual deposits within a year, as they may merge in valley bottoms, such as in narrow channels where debris accumulates; from this perspective, SAFE estimates are conservative. However, SAFE performed well in identifying critical areas with deposits, as demonstrated by a POD of 0.89 and a PPV of 0.67. This suggests that while SAFE may overestimate the total number of avalanches, the detected spatiotemporal trends and patterns remain representative of actual avalanche activity. Another important point is that SAFE mostly detects the latest deposits every year, which are typically wetter deposits. Because SAFE cannot detect early, drier deposits, this limitation must be considered in the interpretation of trend detection results. Our results on wet avalanches are aligned with reports showing or projecting increasing wet avalanche activity globally and in Ladakh (Ballesteros-Cánovas et al., 2018; Eckert et al., 2024; Lavigne et al., 2015). However, occurrence patterns of dry avalanches require further investigation. Moreover, in the many catchments where multivariate regression could not explain changes in avalanche deposits, other variables such as topography (Lied & Bakkehøi, 1980), shifts in liquid-solid precipitation (Eckert et al., 2024), snowpack stability indices (Schweizer et al., 2003), or diurnal temperature changes (Köhler et al., 2018) may help elucidate such trends.

4.2. The First-Order Estimate of Impacts to Snow Avalanches in HMA

In HMA, human lives are directly at risk in homes or while traveling and livelihoods are indirectly affected by snow avalanches where buildings are destroyed or damaged, roads are frequently blocked. In this study, through the overlap of infrastructure with deposit maps (Figure 7), we provided a first-order estimate of impacts on HMA infrastructure and mountain communities for the risk of snow avalanches. Risk is prevalent throughout HMA, particularly in the north, with the highest avalanche frequencies in the west, specifically Amu Darya and Indus, including the mountainous Pamir, Hindu Kush, Karakoram, and Himalaya. However, lower exposure to avalanches does not necessarily ensure better infrastructure resilience, such as in Hengduan Shan in Thanlwin or eastern Tien Shan in Junggar where buildings and roads were particularly exposed. Concerns related to these infrastructure vulnerabilities are exemplified because two out of three dedicated research efforts related to snow avalanches led by the HMA scientific community are situated around critical road infrastructure in otherwise sparsely populated areas of the Chinese Tien Shan and Indian western Himalaya, while the other one focuses on the vulnerability of livelihoods and housing infrastructure in remote valleys of Afghanistan (Acharya et al., 2023).

Despite local knowledge of deposit locations, the low occurrence of large events still leads communities to construct buildings in exposed areas due to limited available space. This is associated with the decline in "social memory" related to natural hazards with time (Komac, 2009). Furthermore, the demand for infrastructure and housing has spurred widespread urbanization, even in relatively remote parts of the Hindu Kush Himalayas, where the population growth exceeded 2% during the second half of the 20th century, accompanied by extensive urban sprawl (Papola et al., 2000). This trend further diminishes available land options, pushing settlements onto or proximate to exposed slopes. In susceptible areas at avalanche risk throughout HMA, 14% of the buildings

were erected on hillslopes with 0.3 to nearly one large avalanche per year. Large and low return period avalanches cause fatalities and injure people (Keiler, 2004), especially in the Pamir, Chinese Himalaya, and Karakoram (Acharya et al., 2023). While rare large deposits are acknowledged to pose severe threats to infrastructure, we underscore the disruptive impact of recurring small to medium size avalanche deposits, which hamper traffic and supply flows within these complex mountain systems every winter at approximately the same locations.

An overlooked aspect of livelihood exposure to snow avalanches is food security. In addition to occasional disruptions in food supply (Caiserman et al., 2022) and livestock losses (Acharya et al., 2023), winter deposits on croplands significantly reduce production. In some cases, crops, cereals, and fertile topsoil are obliterated by thousands of cubic meters of snow (Sidle et al., 2023). The reliance of isolated HMA communities on these farms —for example, in Ladakh (Dame, 2018), Wakhan and Pamir (Kreutzmann, 2003), and the Hindu Kush and Himalaya (Hussain et al., 2019)—for food consumption, along with significant contributions of the agriculture sector to the GDP of HMA nations (17% in 2021, World Bank, 2024), exacerbates the impact of snow hazards on the already fragile food security of such mountainous regions. Priority interventions and decisions are urgently needed in HMA, particularly in southeast (Thanlwin) and northwest (from Amu Darya to Junggar) based on the spatial distribution of avalanches to safeguard vulnerable villages, roads, and croplands, utilizing historical avalanche data to inform spatial planning and mitigation measures for protecting critical infrastructure.

4.3. Evidence of Rising Avalanche Activity in Parts of the HMA and Worldwide

Worldwide, slight decreases in avalanche activity due to temporal declines in snow cover have been observed (e.g., in the Rocky Mountains) (Peitzsch et al., 2021). Additionally, in the Vosges Mountains of France, migration of avalanches to higher elevations was also recorded due to increasing temperatures (Giacona et al., 2021). Conversely, our analysis throughout HMA did not find any trends in surface area or elevation distribution of avalanches. Despite demonstrated retreat of the snowline in HMA (Bolch et al., 2019), deposits can still reach the same areas in runout zones because of wetter snow. In the French Alps and Pyrenees, avalanche runout distances have remained stable for 60 years because they are primarily controlled by slope and terrain (Eckert et al., 2010), not only elevation of the origin zones. The temporally stable elevation distribution of deposits in HMA (CV only 5%; Figure 8a) illustrates this point. In contrast to studies in North America and France, our findings show that increasing temperatures and decreasing snowfall do not necessarily decrease the occurrence of snow avalanches, as already noted in the Indian Himalaya (Ballesteros-Cánovas et al., 2018). In our analysis, we found an increase of 2°C in three of the 33 catchments with an increasing number of deposits, an increase of SWE by 5 mm in one, and a decrease of snowfall by −50 mm in two of these catchments from 1990 to 2022, which partially explained the significant increase of the occurrence of avalanche deposits in western HMA. Collectively, these findings indicate that in catchments where deposits increased, warmer and wetter conditions were observed.

The increasing occurrence of wet snow avalanches, and the increase of dry avalanche activity are also predicted because of warmer and wetter snow conditions in the coming century as shown in the Alps using downscaled climate projections (Mayer et al., 2024). This trend appears to be occurring in western HMA where avalanches have increased with time due to wetter and warmer conditions. Wetter conditions in the early winter (November in our study) may destabilize the snowpack due to earlier percolating water than in spring as typically observed (Reuter et al., 2022). HMA is higher in elevation than the European Alps or the Rocky Mountains which may explain the different trends in wet-dry avalanches. While dry avalanches might decrease in lower elevations as already observed in many areas of the world, we did not observe this response in HMA where the impact of climate at higher elevations tends to increase the proportion of wet avalanches (Ballesteros-Cánovas et al., 2018; Eckert et al., 2024; Lavigne et al., 2015). Moreover, shifts toward more liquid than solid precipitation, without the complete disappearance of snow during winter due to the inherently cold temperature regimes of high mountains, are more likely to occur in the coming century as projected in Tien Shan and Pamir (Yang et al., 2025), potentially increasing the occurrence of slush avalanches. The increase of deposits triggered by a shift from snow to rain, documented also in western Himalaya (Hunt et al., 2020), has already occurred in the Indian Himalaya (Ballesteros-Cánovas et al., 2018) where a shift from dry avalanches to more wet avalanches was observed. Moreover, this counterintuitive relationship is also attributed to the stability of the snowpack, where shallow snowpacks tend to be weaker than deeper snowpacks (Marienthal et al., 2015) and weakness favors instability and release of avalanches, especially slabs (Schweizer et al., 2003).

While certain catchments at risk within HMA exhibited notable changes in the number of avalanche deposits, it is noteworthy that 85% of the aggregated 214 catchments did not display discernible trends in avalanche numbers and none of the 214 catchments displayed any trends in surface area or elevation distribution. This lack of patterns relates to the dynamic occurrence of deposits detected as well as to the variability of the snow and temperature variables relevant to avalanche activity, corresponding to relations noted in the Alps (Schirmer et al., 2022), Nepal (Lievens et al., 2019), Tibet (Wen et al., 2024), and in the wider Himalaya-Karakoram (P. Kumar et al., 2019). In other mountain regions, evidence suggests a lack of clear long-term changes in snow avalanche activity, despite the availability of extensive historical data (Fuchs et al., 2015). Based on 49 years of data in Canada (Bellaire et al., 2016), 50 years in Switzerland (Laternser & Schneebeli, 2002), 100 years in Norway (Laute & Beylich, 2017) and Poland (Gądek et al., 2017), no significant temporal trends of avalanches could be discerned. While our study shows limited localized trends in avalanche activity in several catchments of HMA, the overall findings are similar to other mountain regions. This lack of a clear pattern appears to be inherent given the complexity of mountain terrain, avalanche behavior, and climate change.

5. Conclusions

In this study, we show the benefits of using long-term Landsat constellation archives to derive spatial and temporal patterns of snow avalanches across the entire High Mountain Asia. More than 33 years of snow avalanche deposits were mapped across the region facilitating the automatic generation of the initial vulnerability maps for roads, villages, and agricultural lands in all valleys, including remote ones. Given the regular impacts of avalanches on mountainous communities and the need for mitigation measures informed by a quantified understanding of snow hazard distribution, the SAFE maps are made available online (*Data Availability Statement* section).

Moreover, this first-order estimation of avalanche occurrence for three decades provides a basis for detection of temporal trends since the 1990s, consistent with several key weather parameters retrieved from ERA5 products. Although most of the increases in the occurrence of deposits detected here cannot be solely attributed to climate change, they were directly explained by warmer and wetter conditions in 6 catchments localized in western HMA. These few catchments are contained in the Amu Panj and Indus basins, where the impacts of snow avalanches on communities appear to be most pronounced according to SAFE. There, recent and severe snow hazard events were recorded in all catchments where we detected increases in the number of deposits across years. In the Pamir Mountains (Shiveh, Panj, and Wakhan catchments), even relatively large settlements were directly impacted by large avalanches in 2023 causing several fatalities (AsiaPlus, 2023). In the Nuristan Mountains (Pech catchment), dramatic snow avalanches were reported in 2017 causing the loss of hundreds of lives (Bair et al., 2020). In the Ladakh Mountains, where we conclude that a shift from snow to rain contributed to the increase of deposit occurrence (Upper-Indus and Drass-Shingo catchments), a recent survey with local stakeholders indicated that an increasing number of natural hazards, including snow avalanches, have been observed (Bhat et al., 2023), whereas Ladakh frequently experiences avalanche fatalities (A. Singh et al., 2021).

Despite these patterns in western HMA, the variability in avalanche behavior during recent decades across HMA, demonstrated in this study by the absence of clear tendencies in avalanches in 85% of the studied catchments, reinforces the persistent challenges in avalanche forecasting. This challenge was already highlighted at the beginning of the century in the western Himalaya and attributed to the complex variability of snow and climate parameters (Sharma & Ganju, 2000). Very short-term, if not real-time, predictions of avalanches using Early Warning Systems are possible as already being tested at the Salang Pass in Afghanistan and Künes Basin in Chinese Central Tien Shan (Acharya et al., 2023; Hao et al., 2022). However, given the high variability of snow, any medium to long-term prediction of snow hazards in this century remains highly speculative (Strapazzon et al., 2021). Thus, it is crucial to examine avalanches through a long-term historical analysis, as proposed in this study, to improve our spatially explicit knowledge and preparedness of this hazard by developing and implementing proper mitigation measures (Eckert et al., 2024) based on the number and size of deposits repeatedly observed in SAFE at the same locations. In this regard, SAFE provides data-driven insights to help communities anticipate and mitigate avalanche risks.

Conflict of Interest

The authors declare no conflicts of interest relevant to this study.

Data Availability Statement

The 33-year Snow Avalanches Frequency Estimation (SAFE, 1990–2022) dataset for High Mountain Asia generated in this study is available per basin (Turpan, Junggar, Balkhash, Syr Darya, Amu Darya, Tarim, Indus, Ganga-Brahmaputra, and Thanlwin) on the *Figshare* repository: SAFE-HMA, 2026 (Caiserman, 2026). This dataset can be freely used, provided proper citation is given. SAFE script is available at Caiserman (2022).

This study utilized several publicly available datasets accessed through Google Earth Engine. Climate data, including temperature, albedo, snow cover, snowfall, and precipitation were obtained from ee.ImageCollection ("ECMWF/ERA5_LAND/MONTHLY_AGGR") (Sabater, 2019). Snow water equivalent data (band SWE_inst, kg m^{-2}) across HMA were sourced from ee.ImageCollection ("NASA/FLDAS/NOAH01/C/GL/M/V001") (McNally & NASA/GSFC/HSL, 2018). Slope classification was derived from ee.Image ("CGIAR/SRTM90_V4") (Jarvis et al., 2008) to produce the susceptibility area, while basin and catchment boundaries were delineated using ee.FeatureCollection ("WWF/HydroSHEDS/v1/Basins") (Lehner et al., 2008; Lehner & Grill, 2013). Topographic feature classification was performed using projects/sat-io/open-datasets/Geomorpho90m/cti (Amatulli et al., 2020). Satellite imagery was obtained from Landsat missions including ee.ImageCollection ("LANDSAT/LC09/C02/T1_L2") for Landsat 9, ee.ImageCollection ("LANDSAT/LC08/C02/T1_L2") for Landsat 8, ee.ImageCollection ("LANDSAT/LE07/C02/T1_L2") for Landsat 7, and ee.ImageCollection ("LANDSAT/LT05/C02/T1_L2") for Landsat 5. All datasets are freely accessible through the Google Earth Engine platform.

Acknowledgments
The authors wish to express their sincere gratitude to the World Food Program and the World Bank for their support of the Climate Hazard Impact Monitoring and Research Activities (CHIMRA) project and the Assessment of Avalanche Risk to Roads in the Rasht Valley (Tajikistan) project, respectively. These projects provided the essential foundation for the development of this study, enabling its expansion to encompass the entire High Mountain Asia region.

References

Acharya, A., Steiner, J. F., Walizada, K. M., Ali, S., Zakir, Z. H., Caiserman, A., & Watanabe, T. (2023). Review article: Snow and ice avalanches in high mountain Asia—Scientific, local and indigenous knowledge. *Natural Hazards and Earth System Sciences*, *23*(7), 2569–2592. https://doi.org/10.5194/nhess-23-2569-2023

Amatulli, G., McInerney, D., Sethi, T., Strobl, P., & Domisch, S. (2020). Geomorpho90m, empirical evaluation and accuracy assessment of global high-resolution geomorphometric layers. *Scientific Data*, *7*(1), 162. https://doi.org/10.1038/s41597-020-0479-6

Anchang, J. Y., Ananga, E. O., & Pu, R. (2016). An efficient unsupervised index based approach for mapping urban vegetation from IKONOS imagery. *International Journal of Applied Earth Observation and Geoinformation*, *50*, 211–220. https://doi.org/10.1016/j.jag.2016.04.001

AsiaPlus. (2019). *5 million USD allocated for construction avalanche defense works along the Dushanbe-Chanak highway*. Tajikistan News ASIA-Plus. Retrieved from https://asiaplustj.info/en/news/tajikistan/security/20190429/5-million-usd-allocated-for-construction-avalanche-defense-works-along-the-dushanbe-chanak-highway?utm_source=chatgpt.com

AsiaPlus. (2023). *Two killed in Khorog avalanche*. Tajikistan News ASIA-Plus. Retrieved from https://asiaplustj.info/en/news/tajikistan/incidents/20230215/two-killed-in-khorog-avalanche

Bair, E. H., Rittger, K., Ahmad, J. A., & Chabot, D. (2020). Comparison of modeled snow properties in Afghanistan, Pakistan, and Tajikistan. *The Cryosphere*, *14*(1), 331–347. https://doi.org/10.5194/tc-14-331-2020

Ballesteros-Cánovas, J. A., Trappmann, D., Madrigal-González, J., Eckert, N., & Stoffel, M. (2018). Climate warming enhances snow avalanche risk in the Western Himalayas. *Proceedings of the National Academy of Sciences*, *115*, 3410–3415. https://doi.org/10.1073/pnas.1716913115

Bellaire, S., Jamieson, B., Thumlert, S., Goodrich, J., & Statham, G. (2016). Analysis of long-term weather, snow and avalanche data at Glacier National Park, B.C., Canada. *Cold Regions Science and Technology*, *121*, 118–125. https://doi.org/10.1016/j.coldregions.2015.10.010

Bhat, M. S., Khan, A. A., Akbar, M., & Mir, S. (2023). Disaster-development interface and its impact on emerging vulnerability scenario in Ladakh region of northwestern Himalayas. *J Environ Stud Sci*, *13*(2), 253–270. https://doi.org/10.1007/s13412-023-00818-9

Bolch, T., Shea, J. M., Liu, S., Azam, F. M., Gao, Y., Gruber, S., et al. (2019). Status and change of the cryosphere in the extended Hindu kush himalaya Region. In P. Wester, A. Mishra, A. Mukherji, & A. B. Shrestha (Eds.), *The Hindu kush Himalaya assessment: Mountains, climate change, sustainability and people* (pp. 209–255). Springer International Publishing. https://doi.org/10.1007/978-3-319-92288-1_7

Bühler, Y., Bebi, P., Christen, M., Margreth, S., Stoffel, L., Stoffel, A., et al. (2022). Automated avalanche hazard indication mapping on a statewide scale. *Natural Hazards and Earth System Sciences*, *22*, 1825–1843. https://doi.org/10.5194/nhess-22-1825-2022

Bühler, Y., Hafner, E. D., Zweifel, B., Zesiger, M., & Heisig, H. (2019). Where are the avalanches? Rapid SPOT6 satellite data acquisition to map an extreme avalanche period over the Swiss Alps. *The Cryosphere*, *13*, 3225–3238. https://doi.org/10.5194/tc-13-3225-2019

Caiserman, A. (2022). Snow Avalanche Frequency Estimation (SAFE) (Version 1) [Software]. https://zenodo.org/records/6973757

Caiserman, A. (2026). SAFE-HMA per basin (version 2) [Dataset]. *Figshare*. https://doi.org/10.6084/m9.figshare.28869170.v2

Caiserman, A., Sidle, R. C., & Gurung, D. R. (2022). Snow Avalanche Frequency Estimation (SAFE): 32 years of monitoring remote avalanche depositional zones in high mountains of Afghanistan. *The Cryosphere*, *16*(8), 3295–3312. https://doi.org/10.5194/tc-16-3295-2022

Cavalleri, F., Viterbo, F., Brunetti, M., Bonanno, R., Manara, V., Lussana, C., et al. (2024). Inter-comparison and validation of high-resolution surface air temperature reanalysis fields over Italy. *International Journal of Climatology*, *44*(8), 2681–2700. https://doi.org/10.1002/joc.8475

Chen, F., Xie, T., Yang, Y., Chen, S., Chen, F., Huang, W., & Chen, J. (2023). Discussion of the "warming and wetting" trend and its future variation in the drylands of Northwest China under global warming. *Science China Earth Sciences*, *66*(6), 1241–1257. https://doi.org/10.1007/s11430-022-1098-x

Chen, H., Zhao, J., Liang, Q., Maharjan, S. B., & Joshi, S. P. (2022). Assessing the potential impact of glacial lake outburst floods on individual objects using a high-performance hydrodynamic model and open-source data. *Science of the Total Environment*, *806*, 151289. https://doi.org/10.1016/j.scitotenv.2021.151289

Chen, Y., Li, W., Deng, H., Fang, G., & Li, Z. (2016). Changes in central Asia's water Tower: Past, present and future. *Scientific Reports*, *6*(1), 35458. https://doi.org/10.1038/srep35458

Curio, J., Maussion, F., & Scherer, D. (2015). A 12-year high-resolution climatology of atmospheric water transport over the Tibetan Plateau. *Earth System Dynamics*, *6*(1), 109–124. https://doi.org/10.5194/esd-6-109-2015

Dame, J. (2018). Food security and translocal livelihoods in high Mountains: Evidence from Ladakh, India. *Mountain Research and Development*, *38*(4), 310–322. https://doi.org/10.1659/MRD-JOURNAL-D-18-00026.1

Dar, F. A., Ramanathan, A., Mir, R. A., & Pir, R. A. (2024). Groundwater scenario under climate change and anthropogenic stress in Ladakh Himalaya, India. *Journal of Water and Climate Change*, *15*(4), 1459–1489. https://doi.org/10.2166/wcc.2024.307

de Scally, F. A. (1996). Avalanche snow melting and summer streamflow differences between high-elevation basins, Cascade Mountains, British Columbia, Canada. *Arctic and Alpine Research*, *28*(1), 25–34. https://doi.org/10.1080/00040851.1996.12003144

Eckerstorfer, M., Bühler, Y., Frauenfelder, R., & Malnes, E. (2016). Remote sensing of snow avalanches: Recent advances, potential, and limitations. *Cold Regions Science and Technology*, *121*, 126–140. https://doi.org/10.1016/j.coldregions.2015.11.001

Eckerstorfer, M., & Grahn, J. (2021). *Snow avalanche detection using Sentinel-1 in Langtang, Nepal*. NORCE Norwegian Research Centre. https://agris.fao.org/search/en/providers/125335/records/67659918dcae14e823f7a671

Eckert, N., Baya, H., & Deschatres, M. (2010). Assessing the response of snow Avalanche runout altitudes to climate fluctuations using hierarchical modeling: Application to 61 winters of data in France. *Journal of Climate*, *23*(12), 3157–3180. https://doi.org/10.1175/2010JCLI3312.1

Eckert, N., Corona, C., Giacona, F., Gaume, J., Mayer, S., van Herwijnen, A., et al. (2024). Climate change impacts on snow avalanche activity and related risks. *Nature Reviews Earth & Environment*, *5*(5), 1–21. https://doi.org/10.1038/s43017-024-00540-2

Fuchs, S., Keiler, M., & Sokratov, S. (2015). Snow and avalanches. In A. Kääb, C. Huggel, J. J. Clague, & M. Carey (Eds.), *The high-mountain cryosphere: Environmental changes and human risks* (pp. 50–70). Cambridge University Press. https://doi.org/10.1017/CBO9781107588653.004

Gądek, B., Kaczka, R. J., Rączkowska, Z., Rojan, E., Casteller, A., & Bebi, P. (2017). Snow avalanche activity in Żleb Żandarmerii in a time of climate change (Tatra Mts., Poland). *Catena*, *158*, 201–212. https://doi.org/10.1016/j.catena.2017.07.005

Giacona, F., Eckert, N., Corona, C., Mainieri, R., Morin, S., Stoffel, M., et al. (2021). Upslope migration of snow avalanches in a warming climate. *Proceedings of the National Academy of Sciences*, *118*(44), e2107306118. https://doi.org/10.1073/pnas.2107306118

Greene, E., Birkeland, K., Elder, K., McCammon, I., Staples, M., & Don Sharaf, V. (2010). *Snow, Weather, and Avalanches: Observational guidelines for avalanche programs in the United State*. American Avalanche Association. https://www.americanavalancheassociation.org/

Hafner, E. D., Techel, F., Leinss, S., & Bühler, Y. (2021). Mapping avalanches with satellites—Evaluation of performance and completeness. *The Cryosphere*, *15*(2), 983–1004. https://doi.org/10.5194/tc-15-983-2021

Hamm, A., Arndt, A., Kolbe, C., Wang, X., Thies, B., Boyko, O., et al. (2020). Intercomparison of gridded precipitation datasets over a sub-region of the central Himalaya and the Southwestern Tibetan Plateau. *Water*, *12*(11), 3271. https://doi.org/10.3390/w12113271

Hao, J., Mind'je, R., Zhang, X., Wang, Y., Zhou, H., & Li, L. (2022). Implementation of an early warning for snowfall-triggered avalanche to road safety in the Tianshan Mountains. *Cold Regions Science and Technology*, *204*, 103675. https://doi.org/10.1016/j.coldregions.2022.103675

Hao, J., Zhang, X., Cui, P., Li, L., Wang, Y., Zhang, G., & Li, C. (2023). Impacts of climate change on snow avalanche activity along a transportation corridor in the Tianshan Mountains. *International Journal of Disaster Risk Science*, *14*(4), 510–522. https://doi.org/10.1007/s13753-023-00475-0

Heynen, M., Miles, E., Ragettli, S., Buri, P., Immerzeel, W. W., & Pellicciotti, F. (2016). Air temperature variability in a high-elevation Himalayan catchment. *Annals of Glaciology*, *57*(71), 212–222. https://doi.org/10.3189/2016AoG71A076

Hunt, K. M. R., Turner, A. G., & Shaffrey, L. C. (2020). The impacts of climate change on the winter water cycle of the western Himalaya. *Climate Dynamics*, *55*(7–8), 2287–2307. https://doi.org/10.1007/s00382-020-05383-3

Hussain, A., Mahapatra, B., & Rasul, G. (2019). Adaptation in Mountain agriculture: Food security in the Hindu-Kush Himalayan (HKH) Region. In M. Alam, J. Lee, & P. Sawhney (Eds.), *Status of climate change adaptation in Asia and the Pacific* (pp. 211–236). Springer International Publishing. https://doi.org/10.1007/978-3-319-99347-8_10

Jarvis, A., Reuter, H. I., Nelson, E., & Guevara, E. (2008). Hole-filled SRTM for the globe Version 4. https://srtm.csi.cgiar.org

Keiler, M. (2004). Development of the damage potential resulting from avalanche risk in the period 1950–2000, case study Galtür. *Natural Hazards and Earth System Sciences*, *4*(2), 249–256. https://doi.org/10.5194/nhess-4-249-2004

Khadka, A., Wagnon, P., Brun, F., Shrestha, D., Lejeune, Y., & Arnaud, Y. (2022). Evaluation of ERA5-Land and HARv2 reanalysis data at high elevation in the upper Dudh Koshi Basin (Everest Region, Nepal). *Journal of Applied Meteorology and Climatology*, *61*(8), 931–954. https://doi.org/10.1175/JAMC-D-21-0091.1

Köhler, A., Fischer, J.-T., Scandroglio, R., Bavay, M., McElwaine, J., & Sovilla, B. (2018). Cold-to-warm flow regime transition in snow avalanches. *The Cryosphere*, *12*, 3759–3774. https://doi.org/10.5194/tc-12-3759-2018

Komac, B. (2009). Social memory and geographical memory of natural disasters. *Acta Geographica Slovenica*, *49*(1), 199–226. https://doi.org/10.3986/AGS49107

Kreutzmann, H. (2003). Ethnic minorities and marginality in the Pamirian Knot: Survival of Wakhi and Kirghiz in a harsh environment and global contexts. *The Geographical Journal*, *169*(3), 215–235. https://doi.org/10.1111/1475-4959.00086

Kumar, M., Hodnebrog, Ø., Sophie Daloz, A., Sen, S., Badiger, S., & Krishnaswamy, J. (2021). Measuring precipitation in Eastern Himalaya: Ground validation of eleven satellite, model and gauge interpolated gridded products. *Journal of Hydrology*, *599*, 126252. https://doi.org/10.1016/j.jhydrol.2021.126252

Kumar, P., Saharwardi, M. S., Banerjee, A., Azam, M. F., Dubey, A. K., & Murtugudde, R. (2019). Snowfall variability dictates Glacier mass balance variability in Himalaya-Karakoram. *Scientific Reports*, *9*(1), 18192. https://doi.org/10.1038/s41598-019-54553-9

Kumar, S., Srivastava, P. K., & Snehmani. (2017). GIS-based MCDA–AHP modelling for avalanche susceptibility mapping of Nubra valley region, Indian Himalaya. *Geocarto International*, *32*(11), 1254–1267. https://doi.org/10.1080/10106049.2016.1206626

Laternser, M., & Schneebeli, M. (2002). Temporal trend and spatial distribution of avalanche activity during the last 50 years in Switzerland. *Natural Hazards*, *27*(3), 201–230. https://doi.org/10.1023/A:1020327312719

Laute, K., & Beylich, A. A. (2017). Recent and potential future effects of climate change on snow-avalanche activity in western Norway. In *Presented at the EGU General Assembly Conference Abstracts* (p. 3713). Retrieved from https://ui.adsabs.harvard.edu/abs/2017EGUGA..19.3713L/abstract

Lavigne, A., Eckert, N., Bel, L., & Parent, E. (2015). Adding expert contributions to the spatiotemporal modelling of avalanche activity under different climatic influences. *Journal of the Royal Statistical Society Series C: Applied Statistics*, *64*(4), 651–671. https://doi.org/10.1111/rssc.12095

Lawrimore, J., Ray, R., Applequist, S., Korzeniewski, B., & Menne, M. (2016). Global Summary of the Month (GSOM), version 1. https://doi.org/10.7289/V5QV3JJ5

Lehner, B., & Grill, G. (2013). Global river hydrography and network routing: Baseline data and new approaches to study the world's large river systems. *Hydrological Processes*, *27*(15), 2171–2186. https://doi.org/10.1002/hyp.9740

Lehner, B., Verdin, K., & Jarvis, A. (2008). New global hydrography derived from spaceborne elevation data. *Eos, Transactions American Geophysical Union*, *89*(10), 93–94. https://doi.org/10.1029/2008EO100001

Lesiv, M., See, L., Laso Bayas, J. C., Sturn, T., Schepaschenko, D., Karner, M., et al. (2018). Characterizing the spatial and temporal availability of very high resolution satellite imagery in Google Earth and Microsoft Bing Maps as a source of reference data. *Land*, *7*(4), 118. https://doi.org/10.3390/land7040118

Lied, K., & Bakkehøi, S. (1980). Empirical calculations of snow–avalanche run–out distance based on topographic parameters. *Journal of Glaciology*, *26*(94), 165–177. https://doi.org/10.3189/S0022143000010704

Lievens, H., Demuzere, M., Marshall, H.-P., Reichle, R. H., Brucker, L., Brangers, I., et al. (2019). Snow depth variability in the Northern Hemisphere mountains observed from space. *Nature Communications*, *10*(1), 4629. https://doi.org/10.1038/s41467-019-12566-y

Marienthal, A., Hendrikx, J., Birkeland, K., & Irvine, K. M. (2015). Meteorological variables to aid forecasting deep slab avalanches on persistent weak layers. *Cold Regions Science and Technology*, *120*, 227–236. https://doi.org/10.1016/j.coldregions.2015.08.007

Mayer, S., Hendrick, M., Michel, A., Richter, B., Schweizer, J., Wernli, H., & van Herwijnen, A. (2024). Impact of climate change on snow avalanche activity in the Swiss Alps. *The Cryosphere*, *18*(11), 5495–5517. https://doi.org/10.5194/tc-18-5495-2024

McNally, A., & NASA/GSFC/HSL. (2018). GES DISC Dataset: FLDAS Noah Land Surface Model L4 Global Monthly 0.1 x 0.1 degree (MERRA-2 and CHIRPS) (FLDAS_NOAH01_C_GL_M 001). https://doi.org/10.5067/5NHC22T9375G

Negi, H. S., Kumar, A., Kanda, N., Thakur, N. K., & Singh, K. K. (2021). Status of glaciers and climate change of East Karakoram in early twenty-first century. *Science of the Total Environment*, *753*, 141914. https://doi.org/10.1016/j.scitotenv.2020.141914

OpenStreetMap maps. (2024). Roads and buildings shapefiles (version 1) [Dataset]. Retrieved from https://data.humdata.org/organization/hot

Papola, T. S., Richter, J., & Banskota, M. (2000). Growth, poverty alleviation and sustainable resource management in the Mountain areas of south Asia. In *Proceedings of an international conference*. ICIMOD. https://doi.org/10.53055/ICIMOD.351

Peitzsch, E. H., Boilen, S., Logan, S., Birkeland, K., & Greene, E. (2020). Research note: How old are the people who die in avalanches? A look into the ages of avalanche victims in the United States (1950–2018). *Journal of Outdoor Recreation and Tourism*, *29*, 100255. https://doi.org/10.1016/j.jort.2019.100255

Peitzsch, E. H., Pederson, G. T., Birkeland, K. W., Hendrikx, J., & Fagre, D. B. (2021). Climate drivers of large magnitude snow avalanche years in the U.S. northern Rocky Mountains. *Scientific Reports*, *11*(1), 10032. https://doi.org/10.1038/s41598-021-89547-z

Pepin, N., Arnone, E., Gobiet, A., Haslinger, K., Kotlarski, S., Notarnicola, C., et al. (2022). Climate changes and their elevational patterns in the Mountains of the world. *Reviews of Geophysics*, *60*(1), e2020RG000730. https://doi.org/10.1029/2020RG000730

Pepin, N., Bradley, R. S., Diaz, H. F., Baraer, M., Caceres, E. B., Forsythe, N., et al. (2015). Elevation-dependent warming in mountain regions of the world. *Nature Climate Change*, *5*, 424–430. https://doi.org/10.1038/nclimate2563

Reuter, B., Viallon-Galinier, L., Horton, S., van Herwijnen, A., Mayer, S., Hagenmuller, P., & Morin, S. (2022). Characterizing snow instability with avalanche problem types derived from snow cover simulations. *Cold Regions Science and Technology*, *194*, 103462. https://doi.org/10.1016/j.coldregions.2021.103462

Sabater, M. (2019). ERA5-Land monthly averaged data from 1950 to present. *Copernicus Climate Change Service (C3S) Climate Data Store (CDS)*. https://doi.org/10.24381/cds.68d2bb30

Schaerer, P., & McClung, D. (2006). *The avalanche handbook, mountaineers books*. References-Scientific Research Publishing. Retrieved from https://www.scirp.org/reference/referencespapers?referenceid=2024369

Schirmer, M., Winstral, A., Jonas, T., Burlando, P., & Peleg, N. (2022). Natural climate variability is an important aspect of future projections of snow water resources and rain-on-snow events. *The Cryosphere*, *16*(9), 3469–3488. https://doi.org/10.5194/tc-16-3469-2022

Schweizer, J., Bartelt, P., & van Herwijnen, A. (2015). Chapter 12—Snow avalanches. In J. F. Shroder, W. Haeberli, & C. Whiteman (Eds.), *Snow and ice-related hazards, risks, and disasters, hazards and disasters series* (pp. 395–436). Academic Press. https://doi.org/10.1016/B978-0-12-394849-6.00012-3

Schweizer, J., & Jamieson, J. B. (2003). Snowpack properties for snow profile analysis. In *Cold Regions Science and Technology, ISSW 2002: International Snow Science Workshop* (Vol. 37, pp. 233–241). https://doi.org/10.1016/S0165-232X(03)00067-3

Schweizer, J., Kronholm, K., & Wiesinger, T. (2003). Verification of regional snowpack stability and avalanche danger. *Cold Regions Science and Technology*, *37*(3), 277–288. https://doi.org/10.1016/S0165-232X(03)00070-3

Semakova, E., & Bühler, Y. (2017). TerraSAR-X/TanDEM-X data for natural hazards research in mountainous regions of Uzbekistan. *Journal of Applied Remote Sensing*, *11*, 036024. https://doi.org/10.1117/1.JRS.11.036024

Sharma, S. S., & Ganju, A. (2000). Complexities of avalanche forecasting in Western Himalaya—An overview. *Cold Regions Science and Technology*, *31*(2), 95–102. https://doi.org/10.1016/S0165-232X(99)00034-8

Sidle, R. C., Khan, A. A., Caiserman, A., Qadamov, A., & Khojazoda, Z. (2023). Food security in high mountains of Central Asia: A broader perspective. *BioScience*, *73*(5), 347–363. https://doi.org/10.1093/biosci/biad025

Singh, A., Juyal, V., Kumar, B., Gusain, H. S., Shekhar, M. S., Singh, P., et al. (2021). Avalanche hazard mitigation in east Karakoram mountains. *Natural Hazards*, *105*(1), 643–665. https://doi.org/10.1007/s11069-020-04329-6

Singh, D. K., Mishra, V. D., Gusain, H. S., Gupta, N., & Singh, A. K. (2019). Geo-spatial modeling for automated demarcation of Snow Avalanche hazard areas using Landsat-8 satellite images and in situ data. *Journal of the Indian Society of Remote Sensing*, *47*(3), 513–526. https://doi.org/10.1007/s12524-018-00936-w

Stigter, E. E., Wanders, N., Saloranta, T. M., Shea, J. M., Bierkens, M. F. P., & Immerzeel, W. W. (2017). Assimilation of snow cover and snow depth into a snow model to estimate snow water equivalent and snowmelt runoff in a Himalayan catchment. *The Cryosphere*, *11*(4), 1647–1664. https://doi.org/10.5194/tc-11-1647-2017

Strapazzon, G., Schweizer, J., Chiambretti, I., Brodmann Maeder, M., Brugger, H., & Zafren, K. (2021). Effects of climate change on avalanche accidents and survival. *Frontiers in Physiology*, *12*, 639433. https://doi.org/10.3389/fphys.2021.639433

Sun, F., Chen, Y., Li, Y., Duan, W., Li, B., Fang, G., & Li, Z. (2023). Evaluation of multiple gridded snowfall datasets using gauge observations over high mountain Asia. *Journal of Hydrology*, *626*, 130346. https://doi.org/10.1016/j.jhydrol.2023.130346

Sykes, J., Haegeli, P., & Bühler, Y. (2022). Automated snow avalanche release area delineation in data-sparse, remote, and forested regions. *Natural Hazards and Earth System Sciences*, *22*(10), 3247–3270. https://doi.org/10.5194/nhess-22-3247-2022

The Tribune. (2022). *Fence to minimise avalanche risk near Atal Tunnel*. The Tribune. Retrieved from https://www.tribuneindia.com/news/himachal/fence-to-minimise-avalanche-risk-near-atal-tunnel-408729/

Vanselow, K. A., Zandler, H., & Samimi, C. (2021). Time series analysis of land cover change in dry Mountains: Insights from the Tajik Pamirs. *Remote Sensing*, *13*(19), 3951. https://doi.org/10.3390/rs13193951

Van Tilburg, C., Grissom, C. K., Zafren, K., McIntosh, S., Radwin, M. I., Paal, P., et al. (2017). Wilderness Medical Society Practice Guidelines for prevention and management of Avalanche and Nonavalanche Snow burial accidents. *Wilderness and Environmental Medicine*, *28*(1), 23–42. https://doi.org/10.1016/j.wem.2016.10.004

Wen, H., Wu, X., Shu, X., Wang, D., Zhao, S., Zhou, G., & Li, X. (2024). Spatial heterogeneity and temporal tendency of channeled snow avalanche activity retrieved from Landsat images in the maritime snow climate of the Parlung Tsangpo catchment, southeastern Tibet. *Cold Regions Science and Technology*, *223*, 104206. https://doi.org/10.1016/j.coldregions.2024.104206

World Bank. (2015). *Trans-Hindukush road connectivity Project (P145347)*. Ministry of Public Works, Kabul (Afghanistan). Retrieved from https://documents.worldbank.org/en/publication/documents-reports/documentdetail/465951468184176041

World Bank. (2024). *Agriculture, forestry, and fishing, value added (% of GDP) [WWW Document]*. World Bank Open Data. Retrieved from https://data.worldbank.org

Yang, T., Chen, X., Hamdi, R., Li, L., Cui, F., De Maeyer, P., & Duan, W. (2025). Rainfall-Driven extreme snowmelt will increase in the tianshan and Pamir regions under future climate projection. *Journal of Geophysical Research: Atmospheres*, *130*(1), e2024JD042323. https://doi.org/10.1029/2024JD042323

Zanaga, D., Van De Kerchove, R., Daems, D., De Keersmaecker, W., Brockmann, C., Kirches, G., et al. (2022). ESA WorldCover 10 m 2021 v200. https://doi.org/10.5281/zenodo.7254221

Zhou, B., Wang, Z., Shi, Y., Xu, Y., & Han, Z. (2018). Historical and future changes of snowfall events in China under a warming background. *Journal of Climate*, *31*(15), 5873–5889. https://doi.org/10.1175/JCLI-D-17-0428.1

Zimmermann, M., & Keiler, M. (2015). International frameworks for disaster risk reduction: Useful guidance for sustainable Mountain development? *Mountain Research and Development*, *35*(2), 195–202. https://doi.org/10.1659/MRD-JOURNAL-D-15-00006.1